Application of an In-Plane / Out-Of-Plane Interaction Model for URM Infill Walls to Dynamic Seismic Analysis of RC Frame Buildings

Francesco Longo[1] • Lydell Wiebe[2] • Francesca da Porto[1] • Claudio Modena[1]

[1] DICEA Department, University of Padova, Padua, Italy

[2] Department of Civil Engineering, McMaster University, Hamilton, Canada

Francesco Longo, PhD *(corresponding author)*
Via Brigata Julia 41 – 31040 Cusignana (TV) - Italy
francesco.longo@dicea.unipd.it
ORCID ID: 0000-0001-6382-6190

Lydell Wiebe, PhD, Assistant Professor
Department of Civil Engineering, McMaster University
1280 Main Street West, JHE301 - Hamilton ON L8S 4L7
ORCID ID: 0000-0001-9754-0609

Francesca da Porto, PhD, Associate Professor
Dept. of Civil, Environmental, Architectural Eng., University of Padova
Via Marzolo, 9 - 35131 Padova - Italy
ORCID ID: 0000-0002-9346-9902

Claudio Modena, PhD, Professor
Dept. of Civil, Environmental, Architectural Eng., University of Padova
Via Marzolo, 9 - 35131 Padova - Italy
ORCID ID: 0000-0001-7289-6879

Abstract. Experimental tests have shown that unreinforced masonry (URM) infill walls are affected by simultaneous loading in their in-plane and out-of-plane directions, but there have been few attempts to represent this interaction in nonlinear time history analysis of reinforced concrete (RC) buildings with URM infill walls. In this paper, a recently proposed macro-model that accounts for this interaction is applied to the seismic analysis of RC framed structures with URM infill walls representative of Mediterranean building stock and practices. Two RC framed structures that are representative of low and mid-rise residential buildings are analysed with a suite of a bidirectional ground motions, scaled to three different intensities. During the analyses, the in-plane/out-of-plane interaction is monitored, showing that cracking of the infills occurs predominantly by in-plane actions, while failure occurs due to a combination of in-plane and out-of-plane displacements, with the out-of-plane component usually playing the dominant role. Along the frame height, the bottom storeys are generally the most damaged, especially where thin infill walls are used. These results are consistent with observations of damage to URM infill walls in similar buildings during recent earthquakes.

Keywords URM Infill Walls; In-Plane / Out-of-Plane Interaction; Infilled RC Frames; Nonlinear Time History Analysis;

1. Introduction

Reinforced concrete (RC) framed structures with unreinforced masonry (URM) infill walls are a common building design solution in many countries, especially for low- and mid-rise buildings, because of their reliability against fire and moisture, good thermal and acoustic insulation, and low construction costs. These masonry infill walls can have both positive and negative effects on the global seismic response of RC structures. With a regular distribution of the panels in the frame, infill walls can provide a structure with extra stiffness and strength during an earthquake (Dolšek and Fajfar 2008) and reduce the global displacement demand by increasing the energy dissipation capacity (Ozkaynak et al. 2013). Conversely, other researchers have highlighted both the intrinsic deficiencies of URM infill walls even during minor earthquakes (Calvi et al. 2004) and their detrimental effects on the overall performance of the RC structures (Haldar et al. 2012), consisting of damage and even collapse of both the panels and the RC elements. Some researchers have even concluded that, when significant seismic action is to be expected, masonry infill walls should not be used unless they are specifically designed to work in conjunction with the frame to resist the lateral loads, or remain isolated from the frame (Murty et al. 2006), both requirements that are rarely fulfilled in current practice. Indeed, novel construction systems for masonry infill walls with these features are being developed only lately (Markulak et al. 2013; Mohammadi et al. 2010; Totoev 2015; Preti et al. 2015; Nasiri and Liu 2016) and, more systematically, in the framework of a recently funded European project (da Porto et al. 2016).

In contemporary design practice, masonry infill walls are frequently excluded from the computational models for two main reasons. First, panels are considered non-structural elements in most design guidelines, even though it is now well recognized that infill walls can behave structurally during an earthquake (Fardis and Panagiotakos 1997; Luca et al. 2013). Second, there is a lack of practical modelling tools to represent their complex physical and behavioural nature, including the properties of the brittle materials, the conditions at the interfaces between the infill walls and structural elements, the stiffness of the infill wall relative to that of the bare RC frame, and the rapid degradation of the stiffness and strength that follow cracking and failures of the URM infill walls (Asteris et al. 2013).

Since the 1960s, with the aim of correctly simulating the response of structures with masonry infill walls, two main modelling approaches have emerged: micro-models and macro-models (Crisafulli et al. 2000). Micro-models (Asteris et al. 2013) involve non-linear finite element modelling of the RC frame, the infill panels and the interface between the frame and the wall. Even though this type of model can be most accurate, there are several drawbacks to their implementation and use, mainly related to their complexity and the associated

computational time. Macro-models, on the other hand, are relatively simple analytical models that can simulate the overall wall force-deformation behaviour obtained from experimental results (Lam et al. 2003). Macro-models of URM infill walls, most commonly consisting of single- or multiple-strut models (Asteris et al. 2011), require less computational power during analyses and are therefore more suitable to represent the global behaviour of whole structures. In the most traditional form, a URM infill wall is represented by a pin-jointed diagonal strut made of the same material and having the same thickness as the infill panel. This simulates the in-plane effects of the panel on the surrounding frame, but very seldom is the OOP response incorporated in the computational model. Recently, a few macro-models for the three-dimensional behaviour of URM infill walls have been developed and shown to be less computationally demanding compared to micro-models. However, there is a lack of application of these models to the dynamic seismic response history analysis of realistic structures.

In critical analyses of the damages caused by earthquakes to buildings, RC frames with URM panels have been identified as a source of the high economic losses and sometimes connected with the loss of human lives (Murty et al. 2006). The observed damage usually concerned the infill walls, rather than structural RC frame members. Multiple failure mechanisms have been observed in URM infill walls under earthquake action, including both in-plane (IP) mechanisms and out-of-plane (OOP) collapse. Even though the OOP collapse of masonry panels has been reported in many post-earthquake reconnaissance inspections, there are fewer studies dedicated to OOP behaviour of masonry infill walls under seismic action compared to those regarding the IP behaviour, and only a subset have examined the interaction between the IP and the OOP responses of the walls.

The purpose of this study is to investigate whether a simple numerical model can realistically capture the seismic response of URM infill walls in RC framed structures when the infill wall behaviour is characterized by damage and failures induced by a combination of IP and OOP actions. A URM infill macro-model capable of capturing the interaction between in-plane and out-of-plane response is calibrated and the calibrated macro-elements are used in the numerical models of RC framed structures, with frame configurations representative of the Italian building stock. These realistic infilled frames are analysed with a suite of bidirectional ground motions that are scaled to be compatible with Eurocode 8 elastic spectra. The IP and OOP forces and displacements of the infill walls are monitored to identify when cracking and collapse occur, as well as which panels are most susceptible to damage.

2. Out-of-plane behaviour of URM infill framed walls and interaction

2.1. Observation from past earthquakes

The performance of RC framed structures with masonry infill walls under seismic action has been frequently discussed following many past earthquakes: Northridge (1994) in the U.S.A. (Bruneau 1995), Kocaeli (1999) in Turkey (Dolšek and Fajfar 2001), Abruzzo (2009) (EERI 2009) in Italy, to cite only a few. Even when a seismic event has a relatively low intensity, the most frequent type of damage that affects RC buildings involves the infill masonry walls (Decanini et al. 2004), with the panels at the lower stories often being the most affected (Dolšek and Fajfar 2001). In particular, at early stages of a seismic event URM infill walls can detach from the surrounding frame following the IP displacement demand dictated by the frame structure. Unfortunately, poor conditions between the panels and the surrounding RC frame have long been recognized (West 1973) to significantly reduce the OOP strength of URM infill walls, making them vulnerable to OOP expulsion when subjected to the component of the seismic excitation acting orthogonally to the panels. The vulnerability of masonry infill walls to seismic actions orthogonal to their plane is even increased by the occurrence of in-plane damage. This type of failure was widely reported in many damage surveys after several recent earthquakes in Italy, like the 2009 Abruzzo earthquake (Liel and Lynch 2009; Vicente et al. 2010; Braga et al. 2010), the 2012 Emilia earthquake (Manfredi et al. 2013) and the 2016 Central Italy earthquake (Vv.Aa. 2017), as shown in Figure 1.

Fig. 1 Examples of out-of-plane collapses of masonry infill walls [from Braga et al. 2010]

2.2. In-plane / Out-of-plane interaction in infill wall behaviour

The great majority of the studies on masonry infill walls concentrated on the response to actions in the in-plane (IP) direction (Mohammad Noh et al., 2017). However, during a ground motion, inertia forces also act in the out-of-plane (OOP) direction and they are transferred across the panels to the surrounding frame system. The OOP response of masonry infill panels has been investigated both analytically and through experimental tests. A concise background of research about the OOP behaviour of URM infill walls can be found in Hashemi and Mosalam (2007). However, studies on the response of infill panels undergoing a combination of in-plane and out-of-plane loadings have been rather limited (Maheri and Najafgholipour 2012). In these studies, the words "combination" and "interaction" have been used interchangeably to describe two different phenomena. The first is the modification, usually degradation, of the behaviour in one of the wall's planes caused by previously accumulated damage in the orthogonal direction. In contrast, the second involves the simultaneous loading of infill panels in both the IP and OOP directions. The two phenomena are distinct, and both can occur during the real seismic loading of a URM infill wall (i.e. an already damaged panel can be subjected to simultaneous IP and OOP loading). However, most studies have considered one of these interaction processes at a time.

The effect of OOP damage on IP strength of masonry was investigated with experimental tests on URM full-scale infilled steel frames by Henderson et al. (1993); the studies were later extended by the same authors (Henderson et al. 2006). They showed that prior OOP damage to the infill reduces the IP initial stiffness, but has limited effect on the IP strength of the wall, even after major cracking in the masonry. Likewise, researchers have studied the OOP behaviour of infills affected by damage caused by previous IP loading (Abrams et al. 1993; Angel et al. 1994; Calvi and Bolognini 2001). In general, deterioration of the OOP strength resulting from IP damage was found more significant, particularly so for the panels that have high slenderness ratio (height to thickness ratio, h/t). Moreover, for the walls that experienced limited levels of preliminary IP loading that caused cracking but still maintained good boundary conditions between infill wall and RC frame, the transverse strength of infill panels was found to be much less impacted.

Flanagan and Bennett (1999) studied the interaction phenomena with a comprehensive series of experimental tests, which comprised IP and OOP uniform lateral load tests, OOP drift tests, sequential tests that considered both IP damage followed by OOP loading and OOP damage followed by IP loading and one test with simultaneous loading in both directions. Most of the tests were performed on fully-scaled walls built with structural 200mm thick clay tile units. The results indicated a substantial difference between the two kinds of

interaction. For specimens affected by prior damage, they confirmed that the primary effect of sequential loading is a loss of stiffness, rather than a loss of strength, particularly at moderate levels of loading. Recent experimental campaigns that considered different building practices and wall properties have confirmed that, in low-slenderness specimens affected by prior IP damage caused by a moderate level of IP drift, the primary effect is a loss of stiffness, with moderate effects on the strength. However, when panels that have high slenderness ratio are tested, or when prior IP damage is caused by a high level of IP drift, the strength can also be significantly affected (Komaraneni et al. 2011; Pereira et al. 2011; da Porto et al. 2013). Moreover, when simultaneous IP/OOP loadings were applied, a marked decrease of the lateral pressure capacity of the wall was observed, even though the system remained reasonably stable overall. The observed reduction was linked to the concurrence of OOP loads producing thrust forces around the panel perimeter and IP loads producing strut forces along the diagonal, which created high vertical compression near the panel base and caused failure of the bottom course tiles.

Hashemi and Mosalam (2007) studied the interaction due to simultaneous bidirectional loading on infill walls using finite element models. In a series of nonlinear static analyses, they were able to replicate the significant reduction of the wall capacity observed by Flanagan and Bennett (1999). They summarized the results of the numerical study with an interaction diagram that showed the reduction of IP force capacity of the infilled RC frame for increasing levels of concurrent OOP force acting on the wall. As shown in Figure 2, interaction curves define the maximum combined normalized IP/OOP actions that the infill walls can sustain in terms of simultaneously applied forces or displacements. Several parameters were found to influence the level of interaction and the shape of interaction curves, including aspect ratio, elastic material properties and the inelastic material properties in tension.

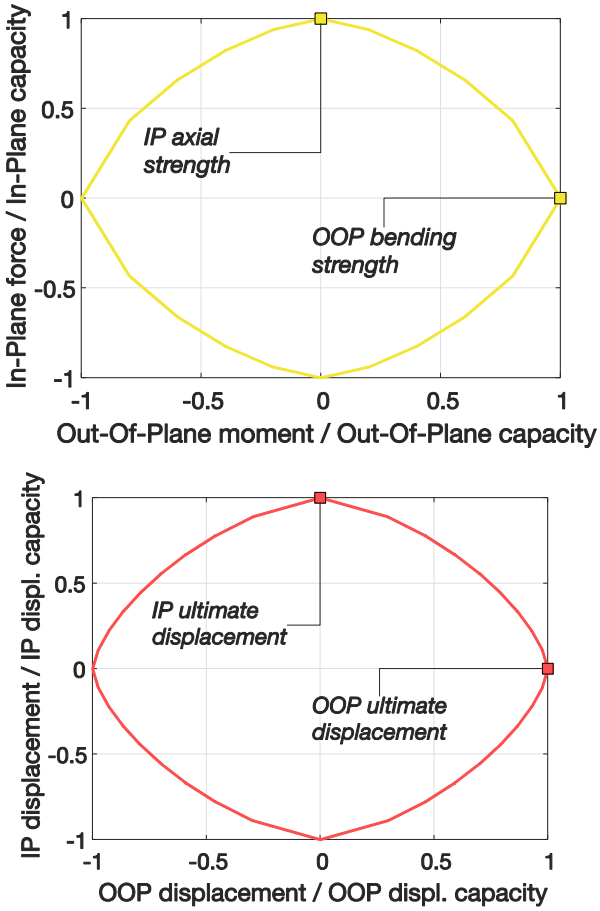

Fig. 2 Examples of interaction curves for URM infill walls. (a) In-Plane / Out-Of-Plane force interaction curve. (b) In-Plane / Out-Of-Plane displacement interaction curve

Recently, many micro-models based on finite element analysis and capable of considering interaction for URM infill walls have been proposed (Kong et al. 2015; Yuen et al. 2016). However, their application is usually limited to the representation of a single infill wall, especially to match experimental results accurately. In order to apply the interaction concept to structural models of buildings, simplified models are preferred, if not required. Hashemi and Mosalam (2007) included the IP/OOP interaction in a numerical macro-model based on two equivalent struts.

Kadysiewski and Mosalam (2009) discussed this model and proposed a different approach with only one equivalent diagonal; their macro-model was then refined and implemented by Mosalam and Günay (2014) and will be described in the next paragraph. Several researchers are developing and refining this approach. Furtado et al. (2015) have also advanced a similar macro-model based on an existing two-diagonal infill wall model (Rodrigues et al. 2010). Di Domenico et. al (2017) proposed empirical formulations for the infill panel's OOP behaviour to improve the agreement between model predictions and experimental data and for alternative IP/OOP interaction expressions. Donà et al. (2017) have presented preliminary findings obtained with a two-

diagonal infill wall model that introduces hysteretic laws to model the degradation of the masonry infill strength and stiffness as a function of the damage level.

Recently, Asteris et al. (2017) performed a comprehensive review of the proposals to include IP/OOP interaction in URM infill walls by using traditional one- or two-diagonal strut models, and suggested modelling the struts as fibre-elements to account explicitly (and not only indirectly) for the arching action effect. The same issue has been also addressed with a proposal by Di Trapani et. al (2018), where the infill wall is modelled with a four- strut macro-element.

3. Analytical model and calibration

3.1. Mosalam and Günay Model

In this paper, the modelling of the URM infill walls follows the proposal by Mosalam and Günay (2014) (MG hereafter), implemented (Günay and Mosalam 2010) in the open source software framework OpenSees (McKenna et al. 2000). In this macro-model (Figure 3), each infill wall is represented with two elastic beam-column elements aligned along one diagonal and with hinges at the extremities. The diagonal elements simulate the IP/OOP interaction of the panels by following two bi-directional domains that govern the yielding criteria and the removal algorithm, respectively. Both elements have a non-linear fibre section at their inner end (i.e. at the central node of the macro-element, where the equivalent mass of the wall is lumped), whereas at the outer extremities they are pinned to the RC frame.

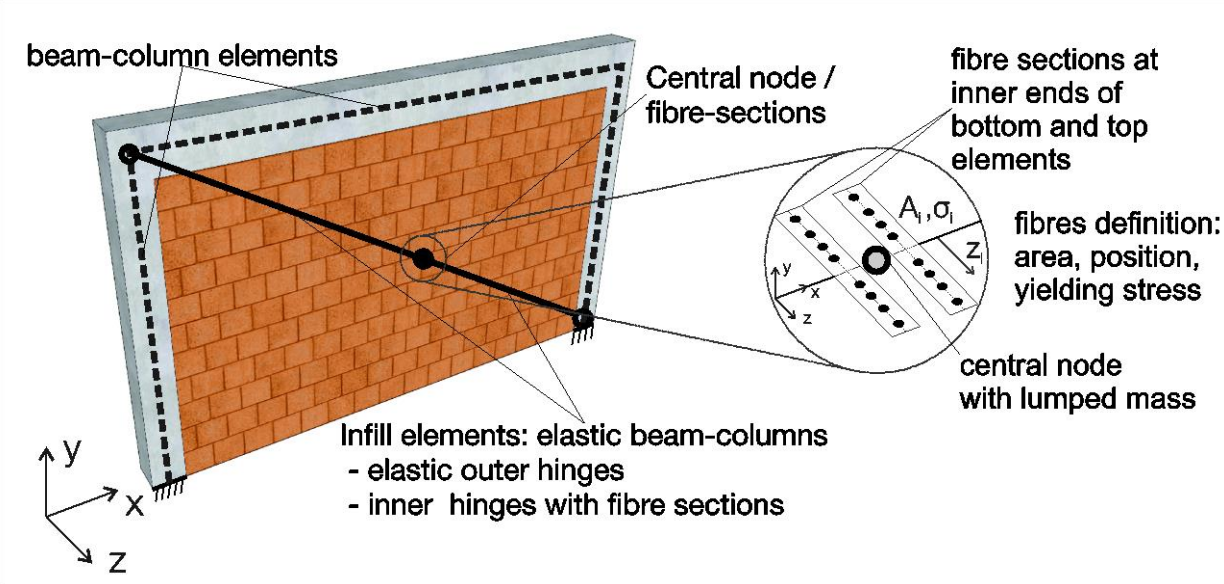

Fig. 3 Schematic representation of the MG model for infill walls with In-Plane/Out-of-Plane interaction

The inertial and mechanical properties of the macro-element are assigned to match those of a suitable equivalent strut. The original MG model follows the FEMA 356 (FEMA 2000) to evaluate the equivalent element area, second moment of inertia, IP axial strength and OOP bending strength. In particular, the width of the equivalent single strut element is evaluated through the formulation proposed by Stafford Smith (1967), in which the parameter λ_h, representing the relative stiffness between the infill and the frame columns, and the ratio between the width w and the length r_w of the equivalent strut, are defined with:

$$\lambda_h = h_c \cdot \sqrt[4]{\frac{E_m t_w \sin 2\theta}{4 E_c I_c h_w}} \qquad (1)$$

$$w/r_w = 0.175 \lambda_h^{-0.4} \quad (2)$$

In Equations (1-2) E_m and E_c are the masonry and concrete moduli of elasticity respectively, I_c and h_c are the moment of inertia and height to the beam centrelines of the column, t_w, h_w and r_w the thickness and height and diagonal length of the infill wall, and θ is the angle whose tangent is the infill height-to-length aspect ratio. These properties are directly assigned to the elastic beam-column elements. The fibre sections at the inner hinges are also modelled to match the same properties; additionally, however, the area, position and strength of the single fibres are manipulated to provide an interaction relationship between the IP and OOP forces. The relationship proposed in the MG model uses a 3/2 power law to link the ratio of the axial strengths at cracking of the infill wall elements with (P_{IP}) or without (P_{IP0}) OOP force, to the bending strengths at cracking with (M_{OOP}) or without (M_{OOP0}) IP force action:

$$\left(\frac{P_{IP}}{P_{IP0}}\right)^{\frac{3}{2}} + \left(\frac{M_{OOP}}{M_{OOP0}}\right)^{\frac{3}{2}} = 1 \quad (3)$$

The model removes wall elements during the analysis if they reach a user-defined envelope combination of IP and OOP displacements. In the absence of more specific test data, Kadysiewski and Mosalam (2009) proposed using the same 3/2 power law to relate combined IP and OOP displacements (Δ_{IP} and Δ_{OOP}, respectively) to the IP and OOP ultimate displacements under unidirectional loading ($\Delta_{IP,u}$ and $\Delta_{OOP,u}$ respectively):

$$\left(\frac{\Delta_{IP}}{\Delta_{IP,u}}\right)^{\frac{3}{2}} + \left(\frac{\Delta_{OOP}}{\Delta_{OOP,u}}\right)^{\frac{3}{2}} = 1 \quad (4)$$

When removal conditions are reached, the equivalent elements, their nodes, the wall mass and associated loads are removed from the model and the analysis continues on the updated model.

Although the MG model accounts for simultaneous IP and OOP actions on the wall, it does not consider degradation of force and displacement capacities due to previous damage accumulated in either the IP or OOP direction. However, Flanagan and Bennett (1999) have concluded that interaction due to simultaneous actions is more significant than that due to sequential applications of loads in two directions. Also, the MG model represents the wall with only one diagonal connecting opposite frame nodes, making it unable to give realistic distributions of bending moments and shear forces in the surrounding RC infilled-frame members. However, as one step towards refining how to properly introduce the phenomena of IP/OOP interaction in URM infill walls under seismic excitation, the focus of this work is on the infill walls rather than the frame members, so the MG model was considered appropriate for this application. Further study is currently underway to develop a comprehensive numerical model for RC frames infilled with masonry walls where both frame and infill wall limit states are considered, and a few interesting preliminary propositions have been cited in Section 2.2.

3.2. Adaptation and model properties adopted for the MG Model

To evaluate design quantities related to the URM infill walls, in this work the provisions of FEMA-356 (FEMA 2000) have been adjusted to Eurocode 6 (CEN 2006) where they differ from the American standard. The axial force capacity of the diagonal beam element, P_{IP0}, which determines the shear strength of the panel, is estimated in accordance with section 6.2 of Eurocode 6:

$$P_{IP0} = \frac{f_{vk}\, t_w l_c}{\gamma_M} \frac{1}{\cos(\theta)} \quad (5)$$

where f_{vk} is the characteristic masonry shear strength, t_w the wall thickness, l_c the compressed wall length, γ_M the material safety factor taken equal to 1, and θ the angle between the beam and the horizontal direction. The out-of-plane capacity of the wall, M_{OOP0} (Equation 6), is extrapolated from the design lateral strength per unit area of wall, q_{lat} , evaluated as shown in Equation 7 (Eurocode 6, Section 6.3.2):

$$M_{OOP0} = \frac{q_{lat} h_w^{\,2} l_w}{8} \quad (6)$$

$$q_{lat} = \frac{f_k}{\gamma_M} \left[\frac{t_w}{h_w} \right]^2 \quad (7)$$

where l_w represents the horizontal length of the infill wall, h_w the wall height and f_k the masonry characteristic compressive strength.

Model calibration was performed by comparing the numerical outputs to available experimental results obtained on two full scale 1 bay - 1 storey planar infilled frames previously tested at University of Pavia (PV) (Calvi and Bolognini 2001) and University of Padova (PD) (da Porto et al. 2013). The experimental setups were tested in the IP direction by applying horizontal displacement cycles with increasing target drifts, and subsequently in the OOP direction by applying the load monotonically. The geometric dimensions, detailing and material properties of the two RC frames were almost identical, and both panels were built with perforated clay units that are commonly found in Italy and other Mediterranean countries, but the infill walls had significantly different thickness and thus slenderness ratios, placing them in the opposing categories of "weak" and "strong" infill walls as defined by other researchers (Uva et. al, 2012). The PV walls were representative of slender "weak" infill panels, which were previously used as a typical partition wall or, albeit less commonly, as a light internal backing wall for outer brick veneer claddings (with the brick veneers often poorly connected to the backing infill wall and commonly attached on-top rather than built in-between the RC frame elements), and are also used as wythe for cavity walls. They were constructed with masonry units measuring 245×245×115 mm in height, length and thickness respectively, with the holes placed horizontally. The PD URM "strong" panels were instead made of thicker clay units with vertical holes, designed to achieve some degree of anti-expulsion resistance even when unreinforced. The masonry units measure 195×240×300 mm, dimensions that are representative of URM blocks currently adopted in newly designed infilled frames. The thickness of horizontal joints was about 10 mm for both the experimental setups. Table 1 summarizes the geometrical and mechanical properties of the walls that were used for the calibration. Data include the height, length and thickness of the URM infills (indicated with h_w, l_w, t_w respectively), the average modulus of elasticity measured between 10% and 40% of the strength, and the average compression strength of the masonry. Both the modulus of elasticity and the compression strength of the masonry were reported both in the direction parallel ($E_{m,//}$, $f_{m,//}$) and perpendicular ($E_{m,\perp}$, $f_{m,\perp}$) to the masonry units holes.

Reinforced concrete frame members were modelled with force-based beam column elements with fibre section discretization (Neuenhofer and Filippou 1998). Both the beams and the columns were modelled in OpenSees with five integration points. A Kent-Scott-Park constitutive relationship (Kent and Park 1971) with added linear tension softening (named Concrete02 in the OpenSees library of materials) was used as the concrete material law. Mander's model (Mander et al. 1988) was adopted to evaluate different material

parameters for plain and confined concrete, based on section transverse detailing. Steel fibres representing the longitudinal reinforcing bars were modelled using a Menegotto-Pinto (1973) model to capture elasto-plastic behaviour and strain-hardening (named Steel02 in the OpenSees library of materials). Comparisons between the experimental data and the numerical analysis output for the in-plane response of PV and PD specimens are shown in Figure 4; in general, good agreement could be obtained between experimental data and numerical results, both for the IP and OOP tests. More details about the calibration were previously discussed elsewhere (Longo et al. 2016).

Table 1 Infill properties of the infill walls tested in Pavia (PV) and Padova (PD) and used for calibration of the model

Test	Direction of construction	h_w (mm)	l_w (mm)	t_w (mm)	$E_{m,\parallel}$ (MPa)	$E_{m,\perp}$ (MPa)	$f_{m,\parallel}$ (MPa)	$f_{m,\perp}$ (MPa)
PV	vertical holes	2750	4200	115	5646	1873	3.97	1.10
	horizontal holes				991		1.11	
PD	vertical holes	2650	4150	300	4312	1767	4.25	0.85

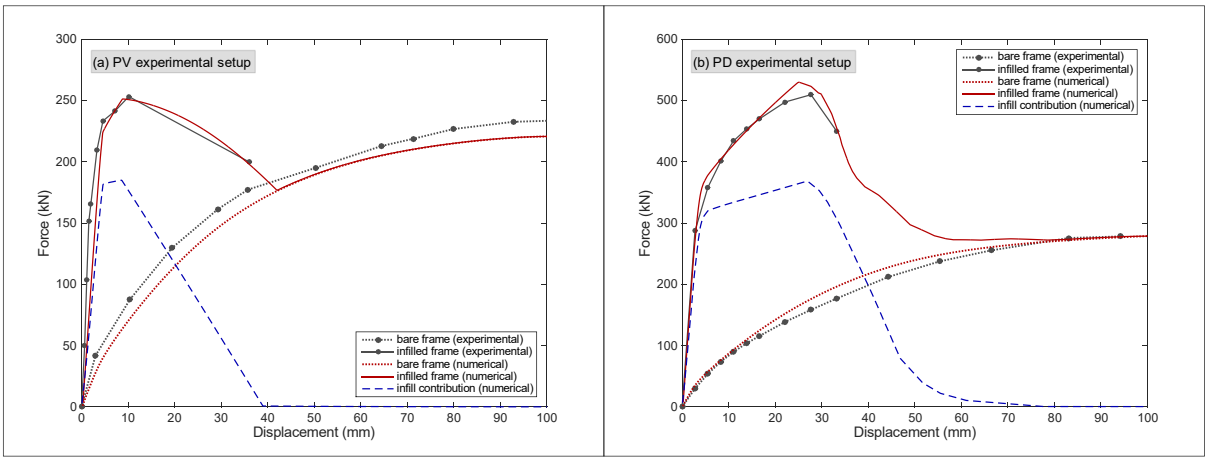

Fig. 4 Comparison between experimental and numerical pushover curves for (a) the PV experimental infilled frame setup (Calvi and Bolognini 2001) and (b) the PD experimental infilled frame setup (da Porto et al. 2013).

4. Analysis of representative infilled frames

4.1. Case Study Buildings

The frame structures are chosen to be representative of the Italian residential building stock, comprising both existing buildings and buildings that could realistically be built according to current design codes. This class of structures is also representative of other Mediterranean countries that share similar building practices. Considering only RC residential buildings in Italy, 95% have five stories or fewer (De Sortis et al. 2007) and

73% have two or three stories (ISTAT 2011). Additionally, Italian residential building stock is relatively aged, especially considering that the first modern seismic-oriented design code became compulsory in 2003 (OPCM 3274 2003): considering only buildings with a reinforced-concrete structure, 67% were built before 1990, and 76% before 2001 (ISTAT 2011). Therefore, currently the majority of Italian RC residential buildings have not been designed with consideration of seismic action. For these reasons, two planar frame configurations with three and five stories were used as analysis models (Figure 5). Both configurations have three bays, with the wider external bays being fully infilled, and the smaller central one without any panel to represent a bay with a wide opening or a staircase. In the following discussion, the models will be designated with 3×3 and 5×3 labels for the configurations with three and five stories, respectively.

In addition, structural RC elements have been modelled to represent two design approaches: "traditional" (T) and "seismic" (S). The traditional design represents most existing structures, which were designed for gravity loads only. Conversely, the seismic approach is the one currently implemented in the Eurocode 8 (CEN 2013) and in the Italian National code (NTC 2008 2008), with specific provisions for lateral loads, ductility and displacement capacity of the elements. In the simplified beam-column modelling technique adopted for this work, the differences in the design approach were introduced through how the fibre sections were discretized and the mechanical properties that were assigned to the elements. Table 2 summarizes the dimensions and detailing of the RC frame members, which are also represented in Figure 6, while Table 3 reports the strength and elastic modulus values of the RC materials.

The frame models were also analysed with both types of infill panels that were previously calibrated, the more slender (115 mm thick) and the thicker (300 mm thick). Hence, combining the two frame configurations (designated with 3×3 and 5×3), the two design approaches (labelled with "T" and "S"), and the two types of infill walls (designated with their thickness, 115 and 300), eight infilled frames models were analysed. Table 4 summarizes the labels that are used to designate the models. The floor height, bay length and infill wall properties were taken close to those of the two calibrated one-bay-one-level laboratory frames because these were similar to the basic building practice rules for infill walls for most Mediterranean countries (Luca et al. 2013).

The ultimate in-plane displacement was set to 1.2% lateral drift, which was the ultimate threshold of the experimental lateral loading setups in the PV and PD frames that were used for calibration. The out-of-plane ultimate displacement was taken equal to 25 mm for both frame typologies, which approximates the average values reached during monotonic OOP loading tests on URM thin/weak infill walls, tested with the same

experimental setup, after a prior in-plane test to 1.2% lateral drift (da Porto et al. 2015). Both values tend to be conservative in the case of thick/strong infill walls; however, in order to facilitate the comparison between the two infill typologies and given the scarcity of available data at the time of these analyses, the same values were adopted for both infill wall types. More recent tests on thick/strong infills (Verlato et al. 2016) have, for example, reached 2.4% in plane drift and, after that level of in-plane drift, achieved out-of-plane displacement of 25-30mm. Despite this simplification, the results presented in Section 5 show that it was still possible to consistently distinguish between the different behaviour of the two types of infill walls, because of the differences in other infill wall characteristics.

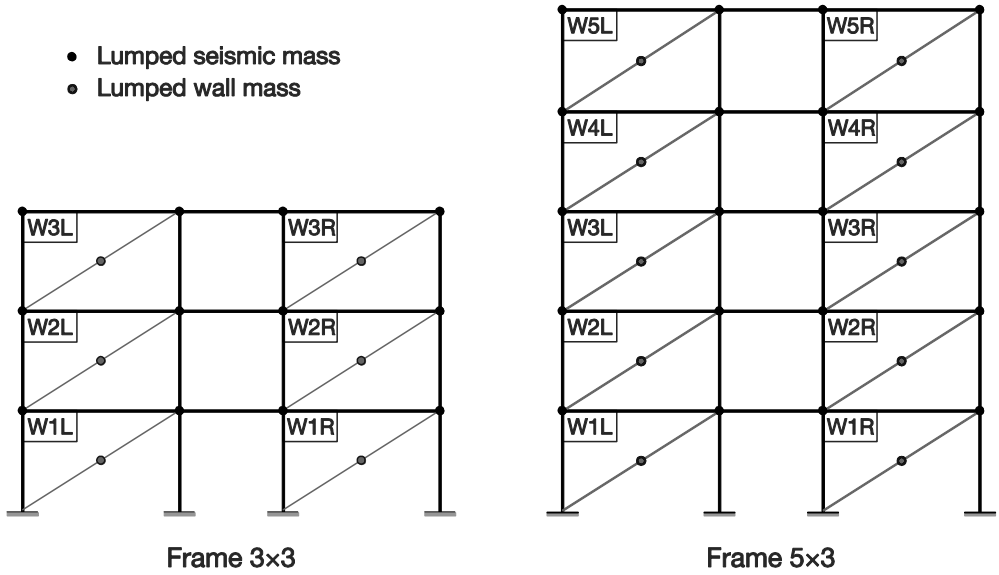

Fig. 5 Schematic representation of the infilled RC planar frames models used in the analyses: 3-storeys and 3-bays (3×3) frame (left) and 5-storeys and 3-bays (5×3) frame (right)

Table 2 Dimensions of RC frames members

Model ID	Columns		Beams	
	Dimensions	Detailing	Dimensions	Detailing
3×3_115T	350×350	Col350T	500×250	BeamT
3×3_300T	350×350			
3×3_115S	350×350	Col350S	300×350	BeamS
3×3_300S	350×350			
5×3_115T	400×400	Col400T	500×250	BeamT
5×3_300T	400×400			
5×3_115S	400×400	Col400S	300×350	BeamS
5×3_300S	400×400			

Table 3 Strength and elastic modulus values of the RC materials

RC design	f_c N/mm^2	E_c kN/mm^2	f_y N/mm^2	E_s kN/mm^2
Traditional (T)	28	26.5	330	200
Seismic (S)	38	30.8	500	200

Table 4 Summary and designations of frame models

Wall thickness	RC design	3 stories and 3 bays	5 stories and 3 bays
135 mm	Traditional	3×3_135T	5×3_135T
	Seismic	3×3_135S	5×3_135S
300 mm	Traditional	3×3_300T	5×3_300T
	Seismic	3×3_300S	5×3_300S

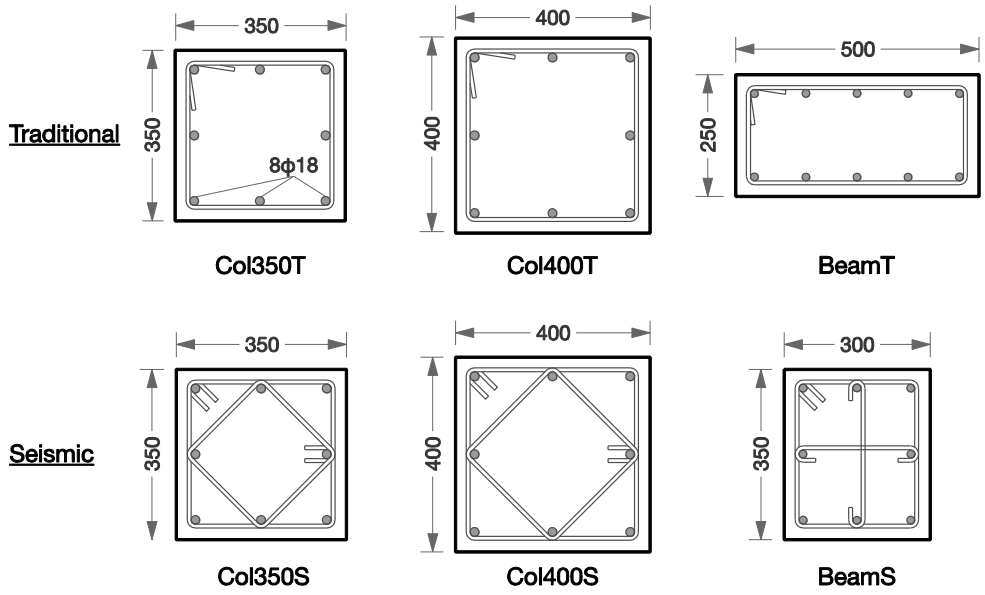

Fig. 6 Traditional and seismic designed RC sections of columns and beams used in planar frames models as listed in Table 2

In order to ensure that the models of the infilled frames had a realistic OOP stiffness, elastic springs with OOP stiffness were assigned to the frame nodes that would connect to beams in the OOP direction (Figure 7). The stiffness values of these springs were calibrated for each model such that the elastic first period of vibration in the OOP direction matched the IP period of the same infilled frame to within a tolerance of 2%, based on the assumption that the actual building would have a similar natural period in both directions. The structural masses of the storeys were lumped at the nodes of each floor level. Tangent stiffness proportional Rayleigh damping (5% of critical) was used, with constants calculated using the first- and third-mode periods.

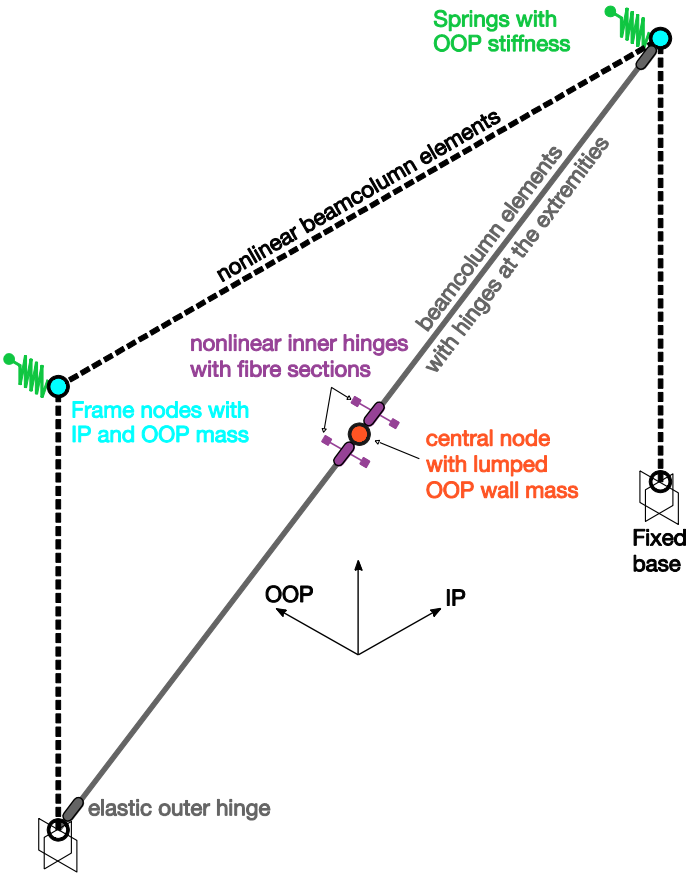

Fig. 7 Computational model with OOP elastic springs

4.2. Bi-directional Ground motion selection

In order to apply simultaneous IP and OOP seismic actions to the models, a bidirectional loading input is required. The general problem of selection and scaling of real records for bi-directional analysis of structures has received numerous contributions (Baker and Cornell 2006; Beyer and Bommer 2006; Shahi and Baker 2013), but there is not yet consensus about the methodology for such a task. This study used the framework and tools described by Iervolino et al. (2008; Iervolino et al. 2011) to build sets of natural records complying with the Eurocode 8 spectra for seismic analysis. Eurocode 8 (CEN 2013) (EC8 hereafter) Type 1 elastic spectra for soil type B (i.e. ground types with shear wave velocity $v_{s,30}$ between 360 and 800 m/s) and 5% viscous damping were chosen as targets for the spectra of the ground motion sets. Specifically, the EC8 spectrum was scaled to three intensity levels, namely $a_g S = 0.15g{\cdot}S$, $0.25g{\cdot}S$ and $0.35g{\cdot}S$, where a_g is the ground acceleration on type A ground (e.g. rock or other rock-like geological formation) and $S = 1.20$ is the soil factor for Type 1 spectrum and ground type B. Processed acceleration time histories and their elastic spectra were taken from the European Strong-Motion database (ESM working group 2015), which comprises historical ground-motion data recorded in the European-Mediterranean and the middle-East regions, and all the records that were selected for the

assembled suite had been processed in the same batch, as described in the database. The database was first filtered to select records that were recorded on sites with a shear velocity within the range for ground type B, with an epicentral distance smaller than 50 km and from earthquakes with moment magnitude Mw > 5.5. This pool of pre-filtered records was then used to build a suite of 20 records: 2 orthogonal horizontal components, from 10 events.

As required by EC8, the records were scaled such that the mean PGA of the scaled set was not less than $a_g \cdot S$, and the mean spectrum was not less than 90% of the target spectrum between $0.2T_1$ and $2T_1$, where T_1 is the fundamental period of the structure in the direction where the accelerogram was to be applied. Additionally, in the final suite, no more than two records were allowed to be taken from any single seismic event. The suite of records was assembled by also aiming to limit the scale factors for the intermediate $0.25g \cdot S$ intensity level to within a factor of 3. The suites for the lower ($0.15g \cdot S$) and higher ($0.35g \cdot S$) intensity levels comprise the same records scaled to match their respective reference spectra, so as to compare the effects on the infill walls for sets of analyses performed at different intensities. As shown in Table 5, the mean scale factors for the three intensity levels are 0.83, 1.38 and 1.93 respectively, and range between 0.28 and 3.90 for any single record. In Figure 8, the elastic spectra of the records are plotted along with the mean spectra of the suite and the reference EC8 spectra. Table 5 summarizes the selected 20 records (the 10 events EQ01-EQ10, times two directions D1 and D2), with their general information from the ESM database, including magnitude, type of fault mechanism, and epicentral distance, stream channel of the record, and peak ground acceleration (PGA).

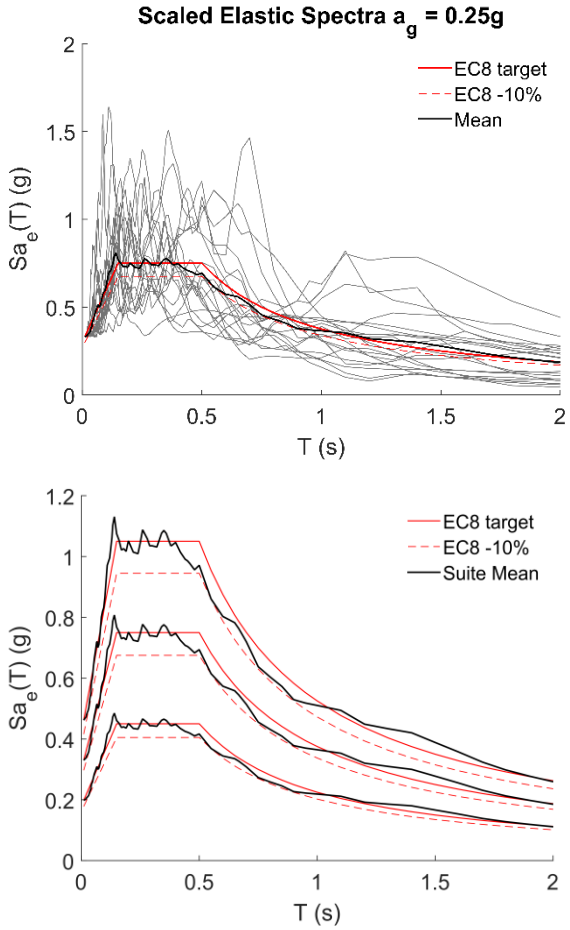

Fig. 8 The suite of ground motion records and comparison between average scaled average spectra and reference EC8 spectra

Table 5 Summary of ground motion suite

Suite ID	Event ID	Date	Station Code	M_W	Style of faulting	R epi. (km)	Stream	PGA (cm/s^2)	Scale factor for $a_g \cdot S$		
									0.15g·*S*	0.25g·*S*	0.35g·*S*
EQ01-D1	IT-1976-0030	15/09/1976	SRC0	6.0	TF	15.8	HNE	-244.9	0.79	1.32	1.85
EQ01-D2	IT-1976-0030	15/09/1976	SRC0	6.0	TF	15.8	HNN	-128.5	1.51	2.52	3.53
EQ02-D1	IS-2000-0053	21/06/2000	109	6.4	SS	18.5	HN2	426.5	0.45	0.76	1.06
EQ02-D2	IS-2000-0053	21/06/2000	109	6.4	SS	18.5	HN3	688.9	0.28	0.47	0.65
EQ03-D1	ME-1979-0012	24/05/1979	BUD	6.2	TF	8.3	HNE	-260.8	0.74	1.24	1.74
EQ03-D2	ME-1979-0012	24/05/1979	BUD	6.2	TF	8.3	HNN	-116.2	1.67	2.79	3.90
EQ04-D1	ME-1979-0003	15/04/1979	ULO	6.9	TF	22.0	HNE	232.3	0.84	1.39	1.95
EQ04-D2	ME-1979-0003	15/04/1979	ULO	6.9	TF	22.0	HNN	277.0	0.70	1.16	1.63
EQ05-D1	IR-1990-0004	20/06/1990	A6211	7.4	SS	34.4	HN2	573.1	0.34	0.56	0.79
EQ05-D2	IR-1990-0004	20/06/1990	A6211	7.4	SS	34.4	HN3	-504.1	0.38	0.64	0.90
EQ06-D1	IT-2009-0009	06/04/2009	AQK	6.1	NF	1.8	HNE	323.7	0.59	0.99	1.39
EQ06-D2	IT-2009-0009	06/04/2009	AQK	6.1	NF	1.8	HNN	-346.8	0.56	0.93	1.30
EQ07-D1	IT-1980-0012	23/11/1980	STR	6.9	NF	33.3	HNE	309.7	0.63	1.04	1.46
EQ07-D2	IT-1980-0012	23/11/1980	STR	6.9	NF	33.3	HNN	-220.9	0.88	1.46	2.05
EQ08-D1	IT-1976-0002	06/05/1976	TLM1	6.4	TF	23.4	HNE	-309.0	0.63	1.05	1.47
EQ08-D2	IT-1976-0002	06/05/1976	TLM1	6.4	TF	23.4	HNN	339.0	0.57	0.95	1.33
EQ09-D1	TK-1999-0077	17/08/1999	4106	7.4	SS	42.8	HNE	-143.6	1.35	2.25	3.15
EQ09-D2	TK-1999-0077	17/08/1999	4106	7.4	SS	42.8	HNN	255.5	0.76	1.27	1.77
EQ10-D1	TK-1999-0415	12/11/1999	9902	7.0	SS	26.5	HNE	121.0	1.61	2.68	3.75
EQ10-D2	TK-1999-0415	12/11/1999	9902	7.0	SS	26.5	HNN	-156.9	1.24	2.06	2.89
								Average	0.83	1.38	1.93

Legend. M_w = Moment magnitude. R epi = Epicentral distance Style of faulting: TF = Thrust faulting; SS = Strike-slip faulting; NF = Normal faulting.

5. Results

5.1. In-Plane / Out-of-Plane force and displacement paths

During the dynamic bi-directional analyses performed on the infilled frame models, the axial loads and the planar displacements of the URM wall correspond to the IP forces and displacements of the equivalent element; likewise, the bending moment / arching action and deflection of the URM wall relate to the OOP bending and displacements on the macro-element. The force and displacement outputs of the element at each time step are represented as force and displacement path histories inside the corresponding interaction curve of the wall. To illustrate the force and displacement paths, the outputs of the two EQ06 records (corresponding to the 2009 Abruzzo earthquake as recorded in L'Aquila) scaled at the intermediate intensity level (a_g=0.25g·S) are shown applied to the frame configurations 3×3_115S and 3×3_300S (Figure 9 and Figure 10, respectively, left column) and 5×3_115T and 5×3_300T (Figure 11 and Figure 12, respectively, left column). These outputs are representative of the results from the other ground motions of the suite for the same scale factor; discussion of the differences between the results from the suite of ground motions will be discussed in the following subsections. In the force paths, the IP and OOP loads are normalized by their respective capacities and plotted on the y- and x-axes, respectively. The plots follow the same arrangement as the infill walls labelled in the planar frames of Figure 5. When an infill wall reaches a combination of IP/OOP forces that yield the fibre sections of the macro-element, cracking is identified and plotted with a dot on the force interaction curve; the time when this occurred is also shown (T_{crk}), enabling the identification of the sequence in which the walls surpassed their strength limit.

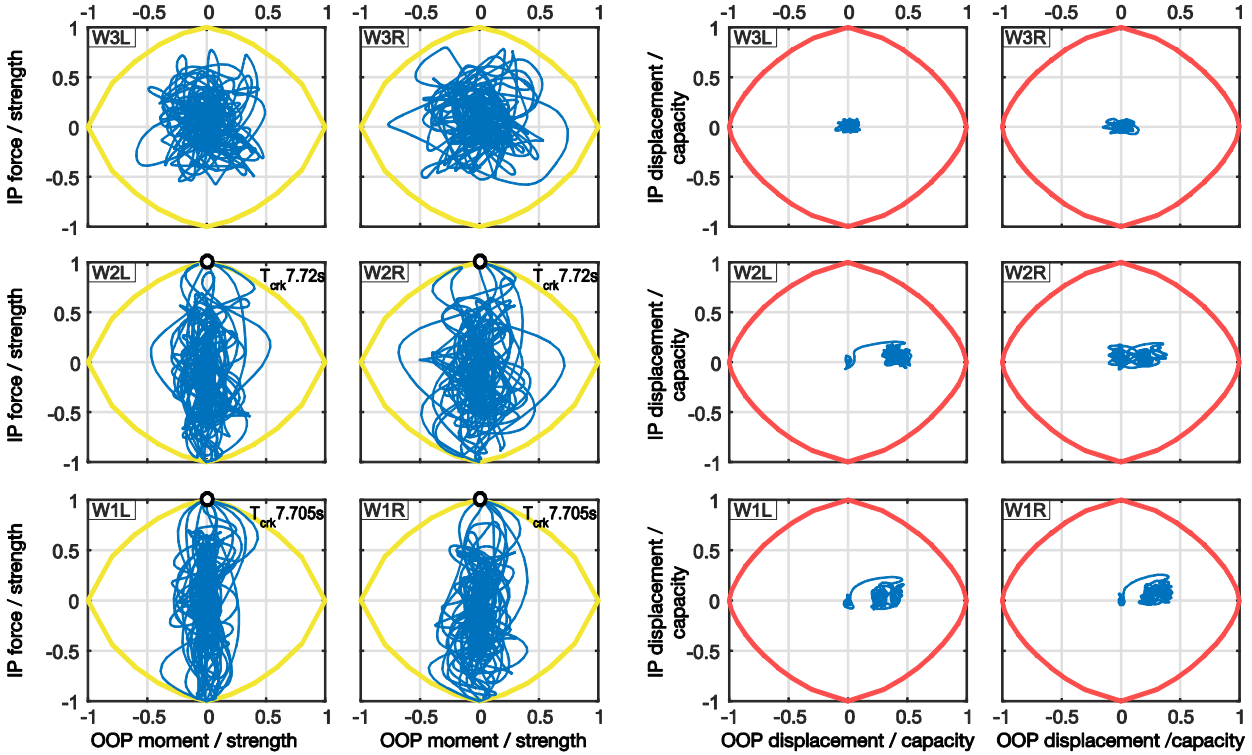

Fig. 9 Force and displacement paths of infill walls in frame **3×3_115S** for analysis EQ06 scaled to a_g = 0.25g

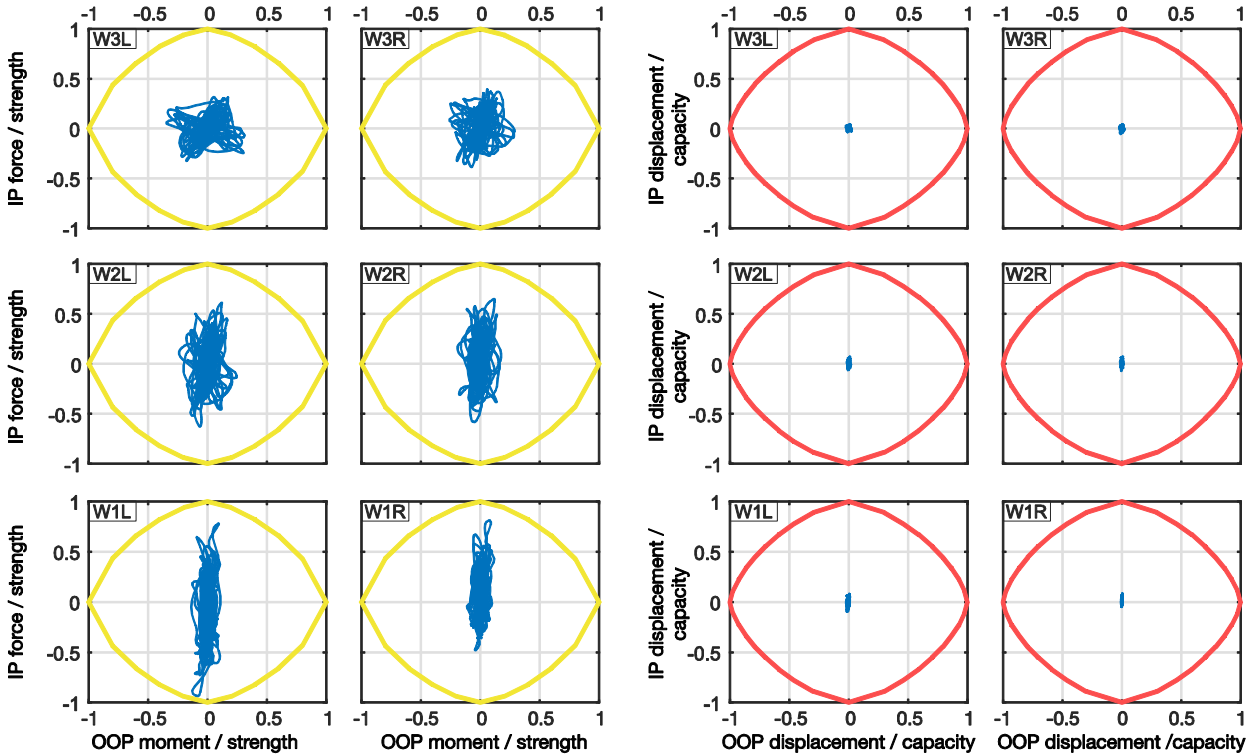

Fig. 10 Force and displacement paths of infill walls in frame **3×3_300S** for analysis EQ06 scaled to $a_g = 0.25g$

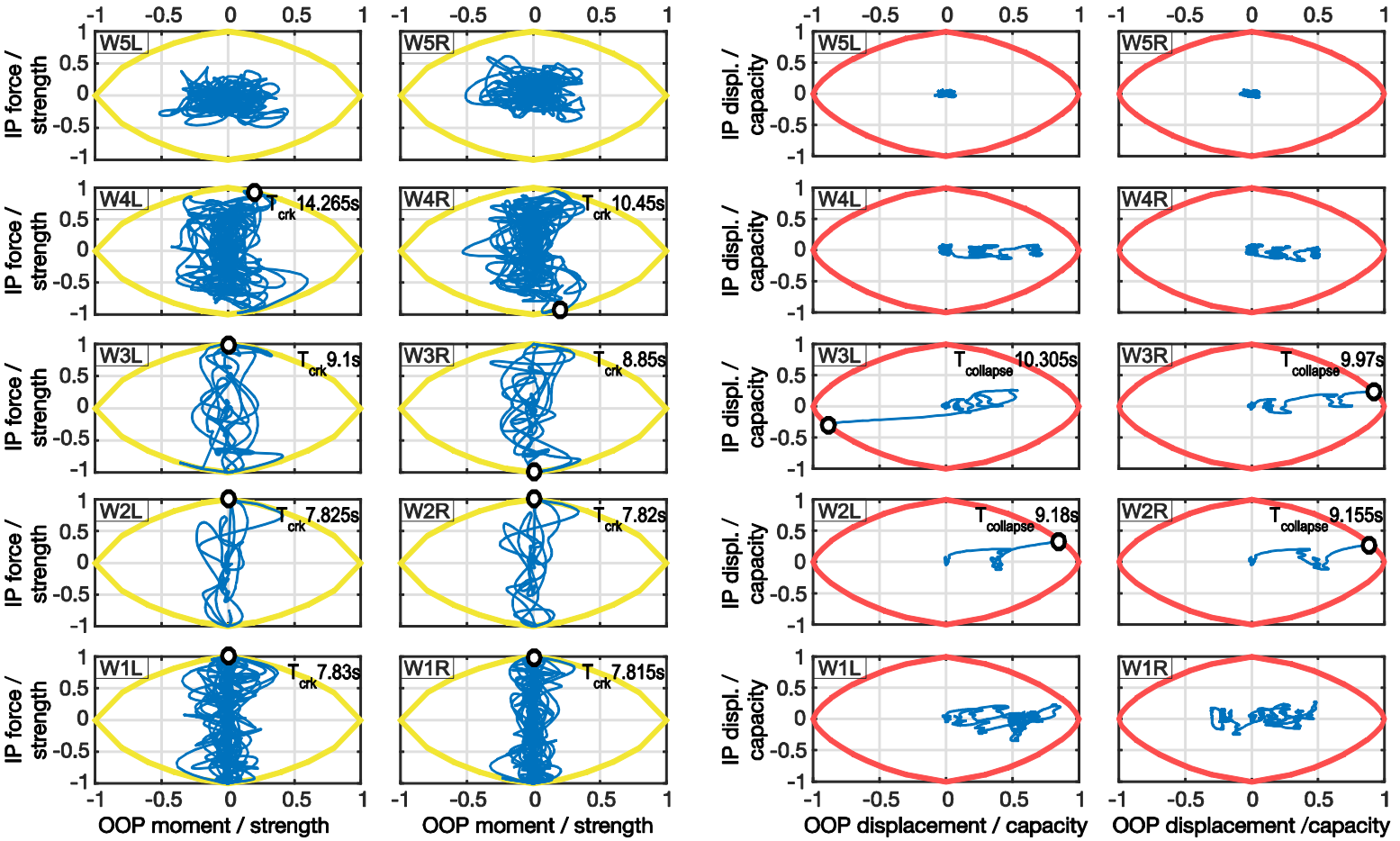

Fig. 11 Force and displacement paths of infill walls in frame **5×3_115T** for analysis EQ06 scaled to a_g = 0.25g

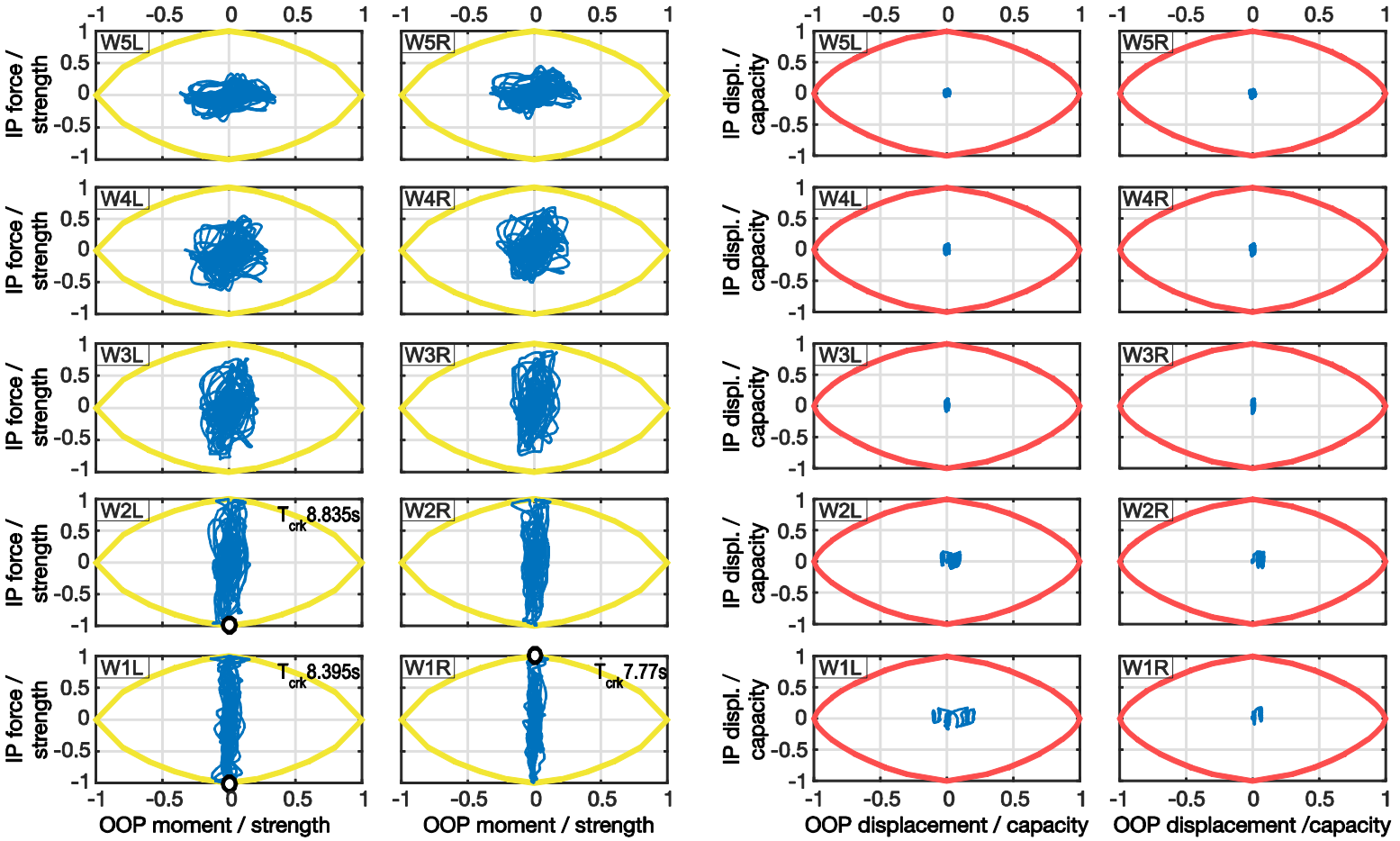

Fig. 12 Force and displacement paths of infill walls in frame **5×3_300T** for analysis EQ06 scaled to $a_g = 0.25g$

Similarly, for the same input ground motions, the right column of Figure 9-12 shows the IP and OOP displacements of the infill walls on the y- and x-axes respectively, along with their displacement capacity domains. The plots show that the displacement levels (both IP and OOP) attained by infill walls before reaching cracking are very small compared to the displacements after cracking has happened: in fact, the displacement path corresponding to analysis points that precede cracking of a wall are concentrated in a small area at the centre of the corresponding displacement envelope. For example, the walls at the third level in Fig. 9, and all of the walls in Fig. 10, do not reach cracking; therefore, the corresponding normalized displacements observed in the IP/OOP envelope curve are very small. Conversely, the displacements of the panels that crack (i.e. those that attain a point in the force/moment interaction curve) tend to increase due to the reduced stiffness. If the infill wall reaches a combination of IP/OOP displacements that exceeds its ultimate capacity, collapse occurs and the corresponding macro-element is removed from the model for the remainder of the analysis. The failure is identified on the plot with a dot and the time of occurrence is shown ($T_{collapse}$), in order to identify the sequence of collapse. Panels that reach cracking do not necessarily collapse. For example, after the walls at the first and second floor in Fig. 9 reach cracking (as is visible in the force/moment domains), their subsequent displacements become significantly higher, but the collapse limit is not reached (as is apparent in the corresponding displacement paths).

The force path series show that walls that do not reach the major cracking threshold are generally loaded to a higher proportion of their in-plane strengths compared to their OOP strengths, as shown by the concentration of the force paths along the vertical axis, particularly at the first and second stories. This trend is stronger for the 300 mm thick walls, which, having a considerably greater OOP stiffness and strength, are subject to smaller OOP demands relative to their capacities. This remains true in spite of the greater mass of the thick walls, which tends to increase the OOP forces. The thinner 115 mm infills reach a more similar proportion of their strengths in the IP and OOP directions, with the force paths in the upper stories occupying the entire force interaction domain almost uniformly. Comparing the force path histories with their corresponding displacement counterparts, it can be seen that panels that do not crack, mostly located at the top stories, maintain displacements that are well below their ultimate displacement limits throughout the analysis.

As a direct consequence of the observed behaviour in the force paths of undamaged panels, panels actually reaching cracking do so with a clear prevalence of in-plane forces caused by the lateral drift of the frame at the lower stories, with the dot indicating panel yielding normally located almost exactly at the IP strength limit without any OOP effects. Moreover, infills where cracking occurs usually have much larger displacements both

IP and OOP, and those that subsequently reach their ultimate displacement capacity do so by a combination of IP and OOP displacements, with the OOP component playing the dominant role. This can be seen by observing in Figure 11 that the dot representing collapse usually has a greater OOP displacement component than IP. Thicker panels, which have significantly higher mass but also significantly higher OOP stiffness, have much smaller displacements and are much less prone to collapse during a given ground motion. Similar results were obtained for most records that were analysed.

The response of the infilled frames is not perfectly symmetric even though the planar frames are, because their computational models are not symmetric, with just one diagonal representing each wall, and also because of the dynamic nature of the loading, with forces and displacements applied to the walls at a given floor not necessarily equal at any given time step, especially in the OOP direction. However, the differences between same-storey walls observed in the force and displacement paths and in the resulting cracked and collapsed panels are overall quite minor, as should be expected for symmetric structures.

5.2. Distribution of damage to URM infill walls in elevation

In order to compare the results from all analyses (EQ01-EQ10) and frame configurations, the URM infill walls were categorized in three classes based on the damage sustained by the end of each analysis: undamaged or lightly damaged (i.e. no cracking registered in model), cracked, or collapsed. The results are shown on the damage grids shown in Figure 13 for the 3×3 frame models and in Figure 14 for the 5×3 frame models. Each grid schematizes a planar frame, with the tiles representing the walls and their colour identifying the damage status at the end of the analysis.

As noted previously for the history paths related to EQ06 analyses, damage to infill walls is notably higher for the thinner URM panels in all the analyses (EQ01-EQ10) and scale factors. This is true for both cracking and collapse. For example, at the lowest intensity level, at least one 115 mm infill wall cracked in almost all analyses, whereas the three-storey frames with 300 mm infill walls avoided cracking in almost all analyses at the lowest intensity level. Additionally, considering all the intensity levels, no wall reached cracking in the top storey of frame configurations 3×3_300 and 5×3_300, whereas cracking of the top panels occurred in about 10% of cases for configurations 3×3_115 and 5×3_115, respectively. When considering collapse, the difference is even more prominent. For example, at the intermediate and highest intensity levels, at least one 115 mm infill wall collapsed in almost all analyses, whereas the 300 mm thick infill walls avoided collapse in all of the three-storey frames and in most of the five-storey frames.

The propensity of lower storeys to sustain damage first, already shown for the path histories of EQ06, is also confirmed throughout the ground motion suite. However, even though damage is clearly concentrated in the lower storeys, the most damaged walls are not necessarily at the lowest levels. This numerical result is seen most clearly in the five-storey frames, in which, out of 47 frames with at least one collapsed wall, 15 did not reach collapse in either wall at the first (ground) storey. Additionally, in the three-storey frames, the same happened in 3 out of 30 frames with collapsed walls. This result is also consistent with observed damage during previous earthquakes (e.g. Figure 1). An explanation for this behaviour is linked to the combined IP/OOP interaction on the walls. The IP forces are proportional to the building lateral drift and therefore generally decrease with increasing elevation. However, the OOP actions on the equivalent elements are proportional to the inertia forces on the walls, which generally increase over the height of the building. Therefore, the effects of the combined actions on the walls can be maximised on a storey higher than the first, even though IP actions would usually dictate the failure of the walls at the lowest level of the building. Moreover, if the combined actions trigger the first collapse on the second-storey walls, the panels at the ground level are even more likely to avoid collapse during the rest of the analysis because a soft storey is created above the first level, prompting a significant reduction in the lateral drift of the first storey. The damage grids show the formation of a soft storey at the second level in several cases (e.g. analyses EQ06 scaled to 0.25g·S and 0.35$g{\cdot}S$ on frame 5×3_115T and EQ10 scaled to 0.25$g{\cdot}S$ on frame 5×3_300T).

Conversely, no evident correlation based on design of the RC members (traditional or seismic) emerges in the distribution of cracked and collapsed walls. On the contrary, case study frames that differed only in RC material properties also show similar history paths, in which the positions of the cracking and collapse dots at each seismic intensity, even if different on analysis-by-analysis basis, follow the same trends for both traditional and seismically designed frames. The apparent small influence of RC member design on the damage sustained by URM infill walls is confirmed by the larger data set represented in the damage grids. For example, as reported in Table 6, there is no strong influence on the number of frames with at least one collapsed wall between traditionally (_T) and seismically (_S) designed RC frames. This result is related to the dominant role of the panels' OOP displacements in the collapse of the URM infill walls, as the OOP displacements are not directly affected by the RC frame members' geometry and detailing, but rather depend on the panel properties and boundary conditions.

Even if the design of the frame has little influence on the behaviour of the infill panels, the panels are expected to have a marked influence on the behaviour of the frame: previous experimental (Manfredi et al.

2015) and numerical (Ricci et al. 2013) studies have shown that both traditionally and seismically designed RC frames are strongly affected by the presence of URM infill walls, even when the panels are uniformly distributed across the RC frame.

Table 6 Number of frames with at least one collapsed wall

$a_g \cdot S$ =	3×3				5×3			
	115T	115S	300T	300S	115T	115S	300T	300S
0.15g·S	0/10	0/10	0/10	0/10	1/10	3/10	0/10	0/10
0.25g·S	6/10	5/10	0/10	0/10	7/10	6/10	2/10	0/10
0.35g·S	9/10	10/10	0/10	0/10	10/10	10/10	4/10	4/10
All	15/30	15/30	0/30	0/30	18/30	19/30	6/30	4/30

The natural ground motion recordings used in the analyses produce variable outcomes in terms of damage to the walls. In this regard, scaling the natural GM records to match the PGA does not provide a particularly good indication of damage levels, but the trends of damage patterns are still clear. Moreover, given the bidirectional nature of the seismic input, the results are also influenced by the orientation of the components in the IP and OOP directions. To address this issue, all of the analyses were repeated with the D1 and D2 components of each ground motion of the suite inverted. Even if different on an analysis-by-analysis comparison, the general trends observed in the force and displacement history paths of the URM infill walls and the observations made based on damage grids in Figures 13-14 were essentially the same. Notwithstanding the influence of dynamic properties of the input ground motions (e.g. frequencies, elastic spectra, soil amplification, etc.) on the damage sustained by the walls, quantifying these influences would require many more analyses and is beyond the scope of this work. However, considering the analyses performed with the whole suite of ground motions that was considered in this research, the results are consistent with experimental results and post-earthquake damage surveys of URM infill walls that were discussed in Section 2. A longer discussion of the results with respect to the variability of ground motion input, along with the detailed results of the analyses with the inverted components, can be found in Longo (2016).

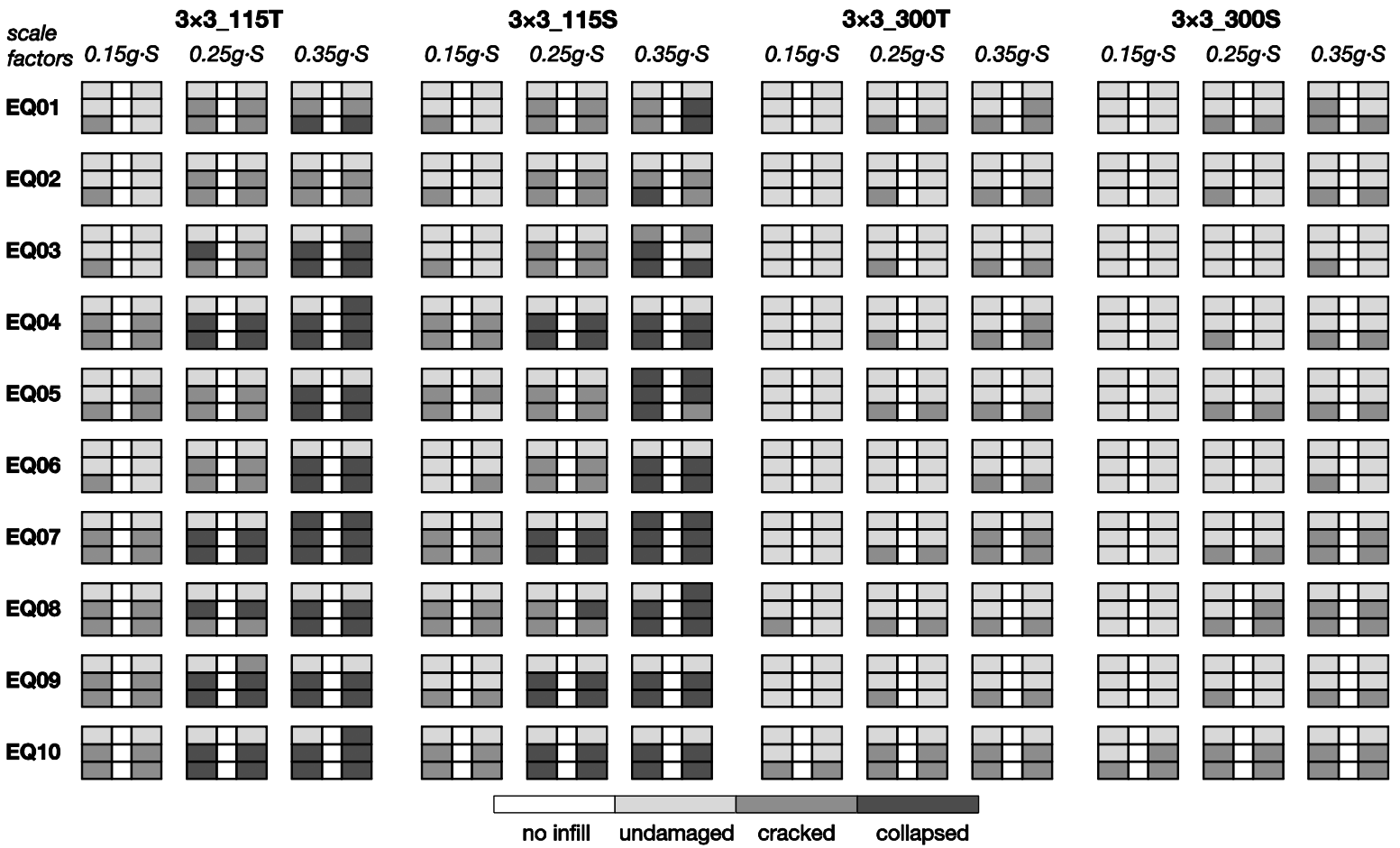

Fig. 13 Damage of the infill walls in the 3×3 frame models at the end of the bi-directional dynamic analyses

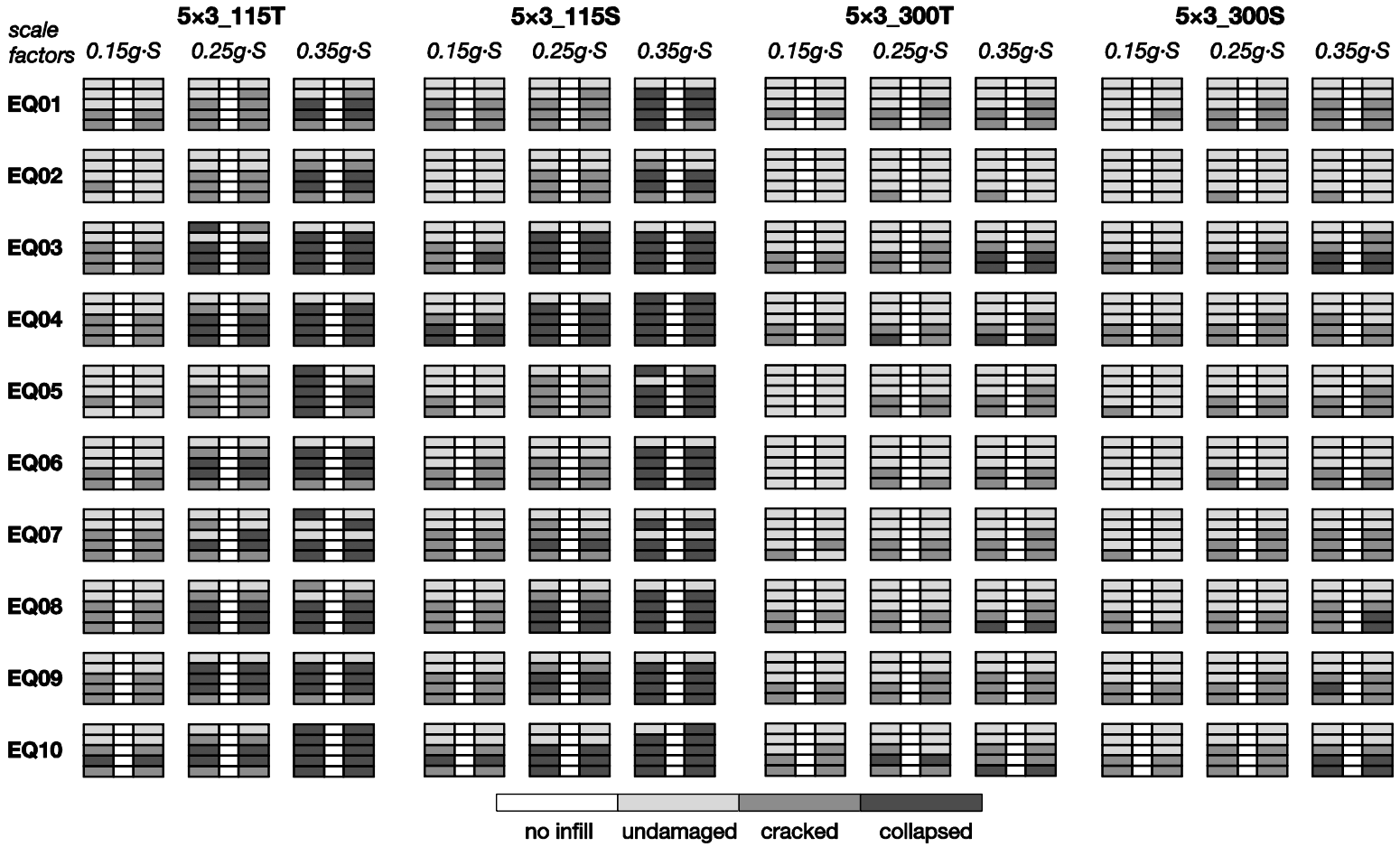

Fig. 14 Damage of the infill walls in the 5×3 frame models at the end of the bi-directional dynamic analyses

5.3. Overall damage condition of the infill walls

Figures 15-16 summarize the results previously displayed on the damage grids, together with the results obtained by rotating the ground motion orientation. Each stacked bar displays the damage condition of all the walls in the frame models at the end of the analysis. In the 3×3 models in Figure 15, this corresponds to 120 walls per bar, while in the 5×3 models in Figure 16 each bar represents 200 walls. To compare the results between different batches of analyses, the bars are normalized by the total number of walls they comprise. The bar plots clearly show that the infill wall typology has the greatest influence on the overall damage to URM infill walls, with slender infill panels being considerably more prone to damage and failure. This is consistent with experimental results on OOP strength of URM infill walls (Dawe and Seah 1989; Abrams et al. 1996). The frequency of cracked slender walls is between 39% and 48% for both the 3×3 and 5×3 models at the $0.15g{\cdot}S$ scale factor, which corresponds to a moderately low design spectrum in many Mediterranean countries. Conversely, at the same scale factor, the 300 mm walls have rates of cracked walls less than 10% and around 24% for the 3×3 and 5×3 configurations, respectively. These results are consistent with the observations of disproportionate damage, and particularly early cracking, to URM infill walls even after relatively low seismic events (Decanini et al. 2004; Penna et al. 2013). Aside from the economic impact, this is particularly concerning because, as shown in the IP/OOP interaction domains, cracked infill walls are far more susceptible to OOP failures, and thus would already be compromised in the event of slightly larger seismic demands or aftershocks.

The behaviour of the two panel typologies is even more distinct when considering the frequency of collapse. The 300 mm infilled structures reach a maximum rate of collapsed walls of about 10% for the five-storey frame configuration at the highest scale factor, and the frequency is less than 1% in the three-storey configuration. For the 115 mm panels, conversely, collapse frequency is between 21% and 39% at the $0.25g{\cdot}S$ scale factor, and between 61% and 72% when scaled to $0.35g{\cdot}S$.

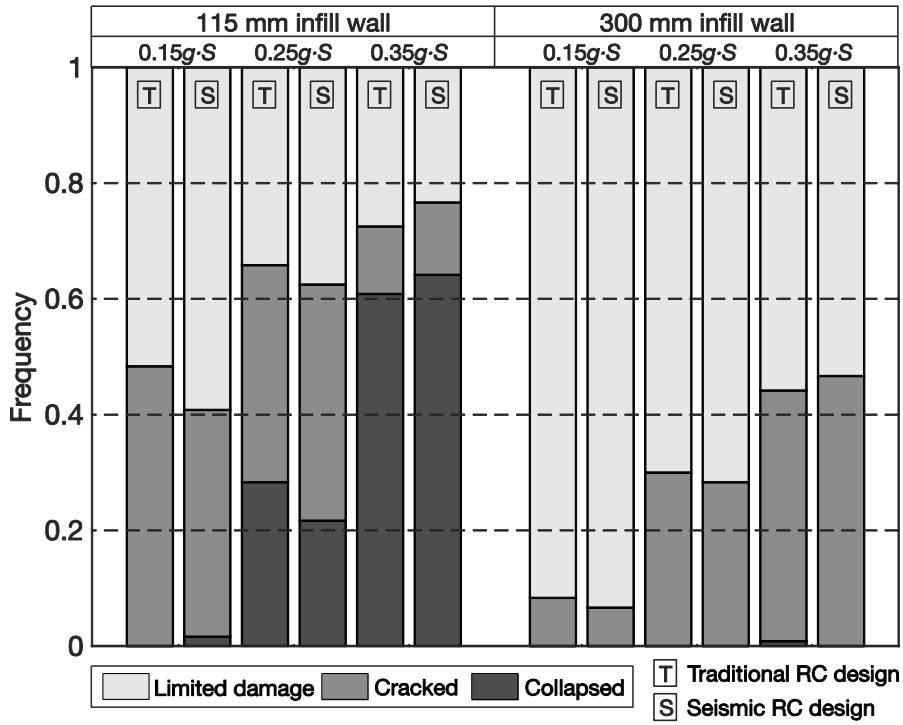

Fig. 15 Frequency of damage to the infill walls at the end of the analyses for 3×3 frame configurations

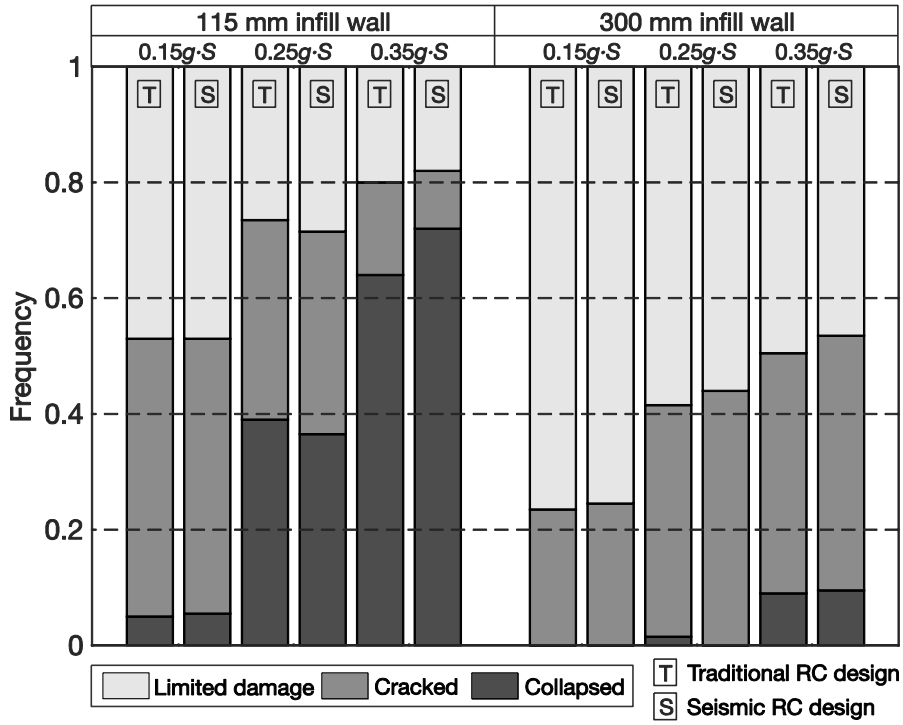

Fig. 16 Frequency of damage to the infill walls at the end of the analyses for 5×3 frame configurations

6. Conclusions

A recently proposed infill wall macro-model that includes in-plane / out-of-plane interaction was applied to the dynamic seismic analysis of a set of realistic RC frame structures. Including simultaneous IP/OOP loading on the response of infill walls during numerical analyses provided results that are neglected by state-of-the-art traditional macro-models that account only for IP behaviour of the panels. The simple infill wall macro-model used in this study was able to capture both interaction phenomena detected in past experimental tests and real observations of damage to URM infill walls in similar buildings in recent earthquakes.

Simultaneous IP/OOP loading has different effects before and after major cracking takes place on the infill walls. Before major cracking, the OOP response of the infills is quite limited, and cracking of the panels is usually dominated by the IP axial force due to frame lateral drift. After major cracking, OOP displacements of the infill walls increase significantly because of the greatly reduced OOP stiffness. Collapses of URM infill walls are governed by a combination of IP/OOP displacements, usually with the OOP components playing the predominant role.

For a given frame configuration and seismic excitation, thinner panels, widely used as enclosures especially in the past, are much more vulnerable to both cracking and collapse compared to the thicker panels that are more common now. However, the RC frame design itself has little influence on the IP/OOP behaviour and damage of URM infill walls.

Both cracking and collapse of the walls tend to happen in the lower stories of the frames first, and then possibly extend to the upper stories. However, upper storeys generally experience only minor damage, except under high intensity ground motions. Even though damage is concentrated in the lower storeys, the most damaged walls are not necessarily at the bottom level. In fact, frames with at least one collapsed wall, but none of them at the first storey, are not uncommon, especially in the taller structures. This result is correlated with the interaction between simultaneous IP and OOP forces and displacements acting on URM infill walls during seismic excitation; this interaction, while supported by increasing experimental evidence, is currently neglected in most design practice.

The simple macro-model used for this work monitors the damage progression of the infill walls with respect to only two thresholds: major cracking of the masonry and collapse. If it were desired to describe the panel response in more detail and with additional significant damage thresholds, to capture specific failure modes (El-Dakhakhni et al. 2003) or damage localization of the URM panels, or to account explicitly for the arching action effect, more detailed computational models and further experimental data about URM infill wall OOP ultimate

displacements would be required. Additionally, the overall interaction could be captured more fully by coupling IP/OOP interaction due to simultaneous loading, which was used in this study, with additional stiffness and strength degradation due to previously accumulated damage in an orthogonal plane. Some recent and still developing proposals, that were referenced in Section 2.2, are currently working to add these enhancements to the infill wall macro-model. This study focused on the damage to the URM infill walls of RC infilled framed structures, assuming for the scope of this work that the infills were more vulnerable than the RC frames. In future work, a state-of-the-art model should also be used for representing the RC frame, so as to understand its interaction with the infill panels under bidirectional loading, including damage and failures that occur in the RC members. It would also be useful to include local effects due to the interaction between the infill walls and the frame members. Also, in this study, calibrated elastic springs were added to the planar frame nodes in order to consider the out-of-plane frame of real buildings. Future research would apply the macro-element model to three-dimensional models of the RC frame buildings, in order to capture the simultaneous inelastic behaviour of panels in both orthogonal directions of the building.

Finally, this study was limited to a set of eight case study planar frames. Future works should include more infill wall thicknesses and typologies, including double leaves clay block, brick and concrete block masonry panels. Additionally, the infill wall model should be applied to a wider range of RC frame structures, including building configurations with a different number of bays and storeys and arrangement of infill walls.

References

Abrams DP, Angel R, Uzarski J (1993) Transverse Strength of Damaged Urm Infills. In: Hamid AA, Harris HG (eds) Proc of 6th North American Masonry Conference. Masonry Society, Philadelphia, pp 347–358

Abrams DP, Angel R, Uzarski J (1996) Out-of-Plane Strength of Unreinforced Masonry Infill Panels. Earthq Spectra 12:825–844. doi: 10.1193/1.1585912

Angel R, Abrams DP, Shapiro D, et al (1994) Behavior of Reinforced Concrete Frames with Masonry Infills. University of Illinois at Urbana-Champaign.

Asteris P, Antoniou S, Sophianopoulos D, Chrysostomou C (2011) Mathematical Macromodeling of Infilled Frames: State of the Art. J Struct Eng 137:1508–1517. doi: 10.1061/(ASCE)ST.1943-541X.0000384

Asteris P, Cavaleri L, Di Trapani F, Tsaris A (2017) Numerical modelling of out-of-plane response of infilled frames: State of the art and future challenges for the equivalent strut macromodels. Eng Struct 132:110–122 . doi: 10.1016/j.engstruct.2016.10.012

Asteris P, Cotsovos DM, Chrysostomou CZ, et al (2013) Mathematical micromodeling of infilled frames: State of the art. Eng Struct 56:1905–1921. doi: 10.1016/j.engstruct.2013.08.010

Baker JW, Cornell CA (2006) Correlation of Response Spectral Values for Multicomponent Ground Motions. Bull Seismol Soc Am 96:215–227. doi: 10.1785/0120050060

Beyer K, Bommer JJ (2006) Relationships between Median Values and between Aleatory Variabilities for Different Definitions of the Horizontal Component of Motion. Bull Seismol Soc Am 96:1512–1522. doi: 10.1785/0120050210

Braga F, Manfredi V, Masi A, et al (2010) Performance of non-structural elements in RC buildings during the L'Aquila, 2009 earthquake. Bull Earthq Eng 9:307–324. doi: 10.1007/s10518-010-9205-7

Bruneau M (1995) Performance of masonry structures during the 1994 Northridge (Los Angeles) earthquake. Can J Civ Eng 22:378–402. doi: 10.1139/l95-048

Calvi GM, Bolognini D (2001) Seismic Response of Reinforced Concrete Frames Infilled with Weakly Reinforced Masonry Panels. J Earthq Eng 5:153–185. doi: 10.1080/13632460109350390

Calvi GM, Bolognini D, Penna A (2004) Seismic performance of masonry-infilled RC frames: Benefits of slight reinforcements. Guimarães, Portugal, pp 253–276

CEN (2006) Eurocode 6: Design of masonry structures - Part 1-1: General rules for reinforced and unreinforced masonry structures. European Committee for Standardization

CEN (2013) Eurocode 8: Design of Structures for Earthquake Resistance - Part 1: General rules, seismic actions and rules for buildings. European Committee for Standardization

Crisafulli FJ, Carr AJ, Park R (2000) Analytical modelling of infilled frame structures: A general review. Bull N Z Natl Soc Earthq Eng 33:30–47.

da Porto F, Guidi G, Dalla Benetta M, Verlato N (2013) Combined In-Plane/Out-of-Plane Experimental Behaviour of Reinforced and Strengthened Infill Masonry Walls. In: Proc. of 12th Canadian Masonry Symposium. The Masonry Society, Vancouver, Canada, p 10

da Porto F, Guidi G, Verlato N, Modena C (2015) Effectiveness of plasters and textile reinforced mortars for strengthening clay masonry infill walls subjected to combined in-plane/out-of-plane actions. Mauerwerk 19:334–354 . doi: 10.1002/dama.201500673

da Porto F, Verlato N, Guidi G, Modena C (2016) The INSYSME project: Innovative construction systems for earthquake resistant masonry infill walls. In: Proceedings of 16th IBMAC (International Brick and Block Masonry Conference. Padova, Italy,

Dawe JL, Seah CK (1989) Out-of-plane resistance of concrete masonry infilled panels. Can J Civ Eng 16:854–864. doi: 10.1139/l89-128

De Sortis A, Bazzurro P, Mollaioli F, Bruno S (2007) Influenza delle tamponature sul rischio sismico degli edifici in calcestruzzo armato. Atti XII Convegno ANIDIS L'ingegneria Sismica Ital Pisa 10–14.

Decanini LD, De Sortis A, Goretti A, et al (2004) Performance of Reinforced Concrete Buildings During the 2002 Molise, Italy, Earthquake. Earthq Spectra 20:S221–S255. doi: 10.1193/1.1765107

Di Domenico M, Ricci P, Verderame G (2017) EMPIRICAL UNREINFORCED MASONRY INFILL MACRO-MODEL ACCOUNTING FOR IN-PLANE/OUT-OF-PLANE INTERACTION. pp 1606–1624

Di Trapani, Shing P. B., Cavaleri L. (2018) Macroelement Model for In-Plane and Out-of-Plane Responses of Masonry Infills in Frame Structures. Journal of Structural Engineering 144:04017198 . doi: 10.1061/(ASCE)ST.1943-541X.0001926

Dolšek M, Fajfar P (2008) The effect of masonry infills on the seismic response of a four-storey reinforced concrete frame — a deterministic assessment. Eng Struct 30:1991–2001. doi: 10.1016/j.engstruct.2008.01.001

Dolšek M, Fajfar P (2001) Soft Storey Effects in Uniformly Infilled Reinforced Concrete Frames. J Earthq Eng 5:1–12. doi: 10.1080/13632460109350383

Donà M, Minotto M, Saler E, et al (2017) Combined in-plane and out-of-plane seismic effects on masonry infills in RC frames. IJEE 34:157–173

EERI (2009) The Mw 6.3 Abruzzo, Italy, Earthquake of April 6, 2009. EERI

El-Dakhakhni WW, Elgaaly M, Hamid AA (2003) Three-Strut Model for Concrete Masonry-Infilled Steel Frames. J Struct Eng 129:177–185. doi: 10.1061/(ASCE)0733-9445(2003)129:2(177)

ESM working group (2015) European Strong-Motion database, version 0.1, Network Activity 3: Networking acceleration networks and SM data users. Project NERA (www.nera-eu.org). http://esm.mi.ingv.it/. Accessed 14 Dec 2015

Fardis MN, Panagiotakos TB (1997) Seismic Design and Response of Bare and Masonry-Infilled Reinforced Concrete Buildings. Part II: Infilled Structures. J Earthq Eng 1:475–503. doi: 10.1080/13632469708962375

FEMA (2000) Prestandard and Commentary for the Seismic Rehabilitation of Buildings. FEMA-356. Federal Emergency Management Agency, Washington, D.C.

Flanagan R, Bennett R (1999) Bidirectional Behavior of Structural Clay Tile Infilled Frames. J Struct Eng 125:236–244. doi: 10.1061/(ASCE)0733-9445(1999)125:3(236)

Furtado A, Rodrigues H, Arêde A, Varum H (2015) Simplified macro-model for infill masonry walls considering the out-of-plane behaviour. Earthq Eng Struct Dyn n/a-n/a. doi: 10.1002/eqe.2663

Günay S, Mosalam KM (2010) Infill Wall Model and Element Removal - OpenSeesWiki. http://opensees.berkeley.edu/wiki/index.php/Infill_Wall_Model_and_Element_Removal. Accessed 27 Feb 2014

Haldar P, Singh Y, Paul DK (2012) Effect of URM infills on seismic vulnerability of Indian code designed RC frame buildings. Earthq Eng Eng Vib 11:233–241. doi: 10.1007/s11803-012-0113-5

Hashemi A, Mosalam KM (2007) Seismic Evaluation of Reinforced Concrete Buildings Including Effects of Masonry Infill Walls. Pacific Earthquake Engineering Research Center, University of California, Berkeley

Henderson RC, Jones WD, Porter ML (1993) Out-of-plane and In-plane Testing of URM Infills. ASCE, pp 1433–1438

Henderson RC, Porter ML, Jones WD, Burdette EG (2006) Influence of Prior Out-of-Plane Damage on the In-Plane Behavior of Masonry Infilled Frames.

Iervolino I, Galasso C, Paolucci R, Pacor F (2011) Engineering ground motion record selection in the ITalian ACcelerometric Archive. Bull Earthq Eng 9:1761–1778. doi: 10.1007/s10518-011-9300-4

Iervolino I, Maddaloni G, Cosenza E (2008) Eurocode 8 Compliant Real Record Sets for Seismic Analysis of Structures. J Earthq Eng 12:54–90. doi: 10.1080/13632460701457173

ISTAT (2011) Censimento delle Popolazione e delle Abitazioni, 2011. http://dati-censimentopopolazione.istat.it/#. Accessed 2 Dec 2015

Kadysiewski S, Mosalam KM (2009) Modeling of Unreinforced Masonry Infill Walls Considering In-Plane and Out-of-Plane Interaction. Pacific Earthquake Engineering Research Center, University of California, Berkeley

Kent DC, Park R (1971) Flexural Members with Confined Concrete. J Struct Div 97:1969–1990.

Komaraneni S, Rai DC, Singhal V (2011) Seismic Behavior of Framed Masonry Panels with Prior Damage When Subjected to Out-of-Plane Loading. Earthq Spectra 27:1077–1103. doi: 10.1193/1.3651624

Kong J-C, Zhai C-H, Liu C-H (2015) Two-way seismic behaviour of concrete frames with infill walls. Proc Inst Civ Eng - Struct Build 168:649–663. doi: 10.1680/jstbu.14.00055

Lam NTK, Griffith M, Wilson J, Doherty K (2003) Time–history analysis of URM walls in out-of-plane flexure. Eng Struct 25:743–754. doi: 10.1016/S0141-0296(02)00218-3

Liel AB, Lynch KP (2009) Vulnerability of reinforced concrete frame buildings and their occupants in the 2009 L'Aquila, Italy earthquake. Natural Hazard Center, Boulder, CO

Longo F (2016) Numerical Modelling of Unreinforced Masonry Infill Walls under Seismic Load Considering In-Plane - Out-Of-Plane Interaction. Ph.D. Thesis, University of Trento

Longo F, Granello G, Tecchio G, et al (2016) A Masonry Infill Wall Model with In-Plane – Out-Of-Plane Interaction Applied to Pushover Analysis of R.C. Frames. In: Proceedings of 16th IBMAC. Padova, Italy,

Luca FD, Verderame GM, Gómez-Martínez F, Pérez-García A (2013) The structural role played by masonry infills on RC building performances after the 2011 Lorca, Spain, earthquake. Bull Earthq Eng 12:1999–2026. doi: 10.1007/s10518-013-9500-1

Maheri MR, Najafgholipour MA (2012) In-Plane Shear and Out-of-Plane Bending Capacity Interaction in Brick Masonry Walls. In: Proc. of 15th World Conference on Earthquake Engineering. Lisbon, Portugal,

Mander J, Priestley M, Park R (1988) Theoretical Stress-Strain Model for Confined Concrete. J Struct Eng 114:1804–1826. doi: 10.1061/(ASCE)0733-9445(1988)114:8(1804)

Manfredi G, Monti G, Spacone E (2015) Reinforced Concrete Structures. In: Manfredi G, Dolce M (eds) The state of Earthquake Engineering Research in Italy: the ReLUIS-DPC 2010-2013 Project. Doppiavoce, Napoli, Italy, pp 1–49

Manfredi G, Prota A, Verderame GM, et al (2014) 2012 Emilia earthquake, Italy: reinforced concrete buildings response. Bull Earthquake Eng 12:2275–2298 . doi: 10.1007/s10518-013-9512-x

Markulak D, Radić I, Sigmund V (2013) Cyclic testing of single bay steel frames with various types of masonry infill. Eng Struct 51:267–277. doi: 10.1016/j.engstruct.2013.01.026

McKenna F, Fenves GL, Scott MH (2000) Open system for earthquake engineering simulation (OpenSees). Pacific Earthquake Engineering Research Center.

Menegotto M, Pinto PE (1973) Method of analysis for cyclically loaded reinforced concrete plane frames including changes in geometry and non-elastic behaviour of elements under combined normal force and bending. In: Proceedings of IABSE Symposium on Resistance and Ultimate Deformability of Structures Acted on by Well Defined Repeated Loads. Lisbon, pp 15–22

Mohammad Noh N, Liberatore L, Mollaioli F, Tesfamariam S (2017) Modelling of masonry infilled RC frames subjected to cyclic loads: State of the art review and modelling with OpenSees. Engineering Structures 150:599–621 . doi: 10.1016/j.engstruct.2017.07.002

Mohammadi M, Akrami V, Mohammadi-Ghazi R (2010) Methods to Improve Infilled Frame Ductility. J Struct Eng 136:646–653.

Mosalam KM, Günay S (2014) Progressive Collapse Analysis of RC Frames with URM Infill Walls Considering In-Plane/Out-of-Plane Interaction. Earthq Spectra. doi: 10.1193/062113EQS165M

Murty CVR, Brzev S, Faison H, et al (2006) AT RISK: The Seismic Performance of Reinforced Concrete Frame Buildings with Masonry Infill Walls. EERI, Oakland, CA

Nasiri E, Liu Y (2016) Experimental study of the effect of interfacial gaps on the in-plane behaviour of masonry infilled RC frames. In: Proceedings of 16th IBMAC (International Brick and Block Masonry Conference. Padova, Italy,

Neuenhofer A, Filippou F (1998) Geometrically Nonlinear Flexibility-Based Frame Finite Element. J Struct Eng 124:704–711. doi: 10.1061/(ASCE)0733-9445(1998)124:6(704)

NTC 2008 (2008) D.M. 14.01.2008 "Nuove Norme Tecniche per le costruzioni".

OPCM 3274 (2003) Opcm n. 3274 del 20 marzo 2003: primi elementi in materia di criteri generali per la classificazione sismica del territorio nazionale e di normative tecniche per le costruzioni in zona sismica.

Ozkaynak H, Yuksel E, Yalcin C, et al (2013) Masonry infill walls in reinforced concrete frames as a source of structural damping. Earthq Eng Struct Dyn 43:949–968. doi: 10.1002/eqe.2380

Penna A, Morandi P, Rota M, et al (2013) Performance of masonry buildings during the Emilia 2012 earthquake. Bull Earthq Eng 12:2255–2273. doi: 10.1007/s10518-013-9496-6

Pereira MFP, Pereira MFN, Ferreira JED, Lourenço PB (2011) Behavior of masonry infill panels in RC frames subjected to in plane and out of plane loads. In: 7th Int. Conf. AMCM2011. Kraków, Poland,

Preti M, Migliorati L, Giuriani E (2015) Experimental testing of engineered masonry infill walls for post-earthquake structural damage control. Bull Earthq Eng 13:2029–2049.

Ricci P, Risi MTD, Verderame GM, Manfredi G (2013) Influence of infill distribution and design typology on seismic performance of low- and mid-rise RC buildings. Bull Earthq Eng 11:1585–1616. doi: 10.1007/s10518-013-9453-4

Rodrigues H, Varum H, Costa A (2010) Simplified Macro-Model for Infill Masonry Panels. J Earthq Eng 14:390–416. doi: 10.1080/13632460903086044

Shahi SK, Baker JW (2013) NGA-West2 Models for Ground Motion Directionality. Earthq Spectra 30:1285–1300. doi: 10.1193/040913EQS097M

Stafford Smith B (1967) Methods for predicting the lateral stiffness and strength of multi-storey infilled frames. Build Sci 2:247–257.

Totoev Y (2015) Classification of SIM infill panels/Klassifikation von SIM-Ausfachungswänden. Mauerwerk 19:74–79.

Uva G, Porco F, Fiore A (2012) Appraisal of masonry infill walls effect in the seismic response of RC framed buildings: A case study. Engineering Structures 34:514–526 . doi: 10.1016/j.engstruct.2011.08.043

Verlato N, Guidi G, da Porto F, Modena C (2016) Innovative systems for masonry infill walls based on the use of deformable joints: Combined in-plane/out-of-plane tests. In: Proceedings of the 16th International Brick and Block Masonry Conference,. Padova, Italy, pp 1359–1366

Vicente R, Rodrigues H, Costa A, et al (2010) Masonry enclosure walls: lessons learnt from the recent Abruzzo Earthquake. In: Proc. of 14th ECEE. Ohrid, Macedonia,

Vv.Aa. (2017) Performance of masonry buildings in the seismic sequence of Central Italy 2016 - Part 1: Overview. Progettazione Sismica 8:49–74 . doi: 10.7414/PS.8.2.49-77

West HWH (1973) Lateral loading test on walls with different boundary conditions. In: Proc. of Third International Brick Masonry Conference. Essen, Germany,

Yuen TYP, Kuang JS, Ali BSM (2016) Assessing the effect of bi-directional loading on nonlinear static and dynamic behaviour of masonry-infilled frames with openings. Bull Earthq Eng 14:1721–1755 . doi: 10.1007/s10518-016-9899-2